RESEARCH ARTICLE

β-Catenin Activation Promotes Immune Escape and Resistance to Anti–PD-1 Therapy in Hepatocellular Carcinoma

Marina Ruiz de Galarreta[1,2,3], Erin Bresnahan[1,2,3], Pedro Molina-Sánchez[1,2,3], Katherine E. Lindblad[1,2,3,4], Barbara Maier[1,3], Daniela Sia[2], Marc Puigvehi[2,5], Verónica Miguela[1,2,3], María Casanova-Acebes[1,3], Maxime Dhainaut[1,3], Carlos Villacorta-Martin[2], Aatur D. Singhi[6,7], Akshata Moghe[6], Johann von Felden[2,8], Lauren Tal Grinspan[1,2,3], Shuang Wang[2], Alice O. Kamphorst[1,3,4], Satdarshan P. Monga[6,7], Brian D. Brown[3,4], Augusto Villanueva[2,4], Josep M. Llovet[2,9,10], Miriam Merad[1,3,4], and Amaia Lujambio[1,2,3,4]

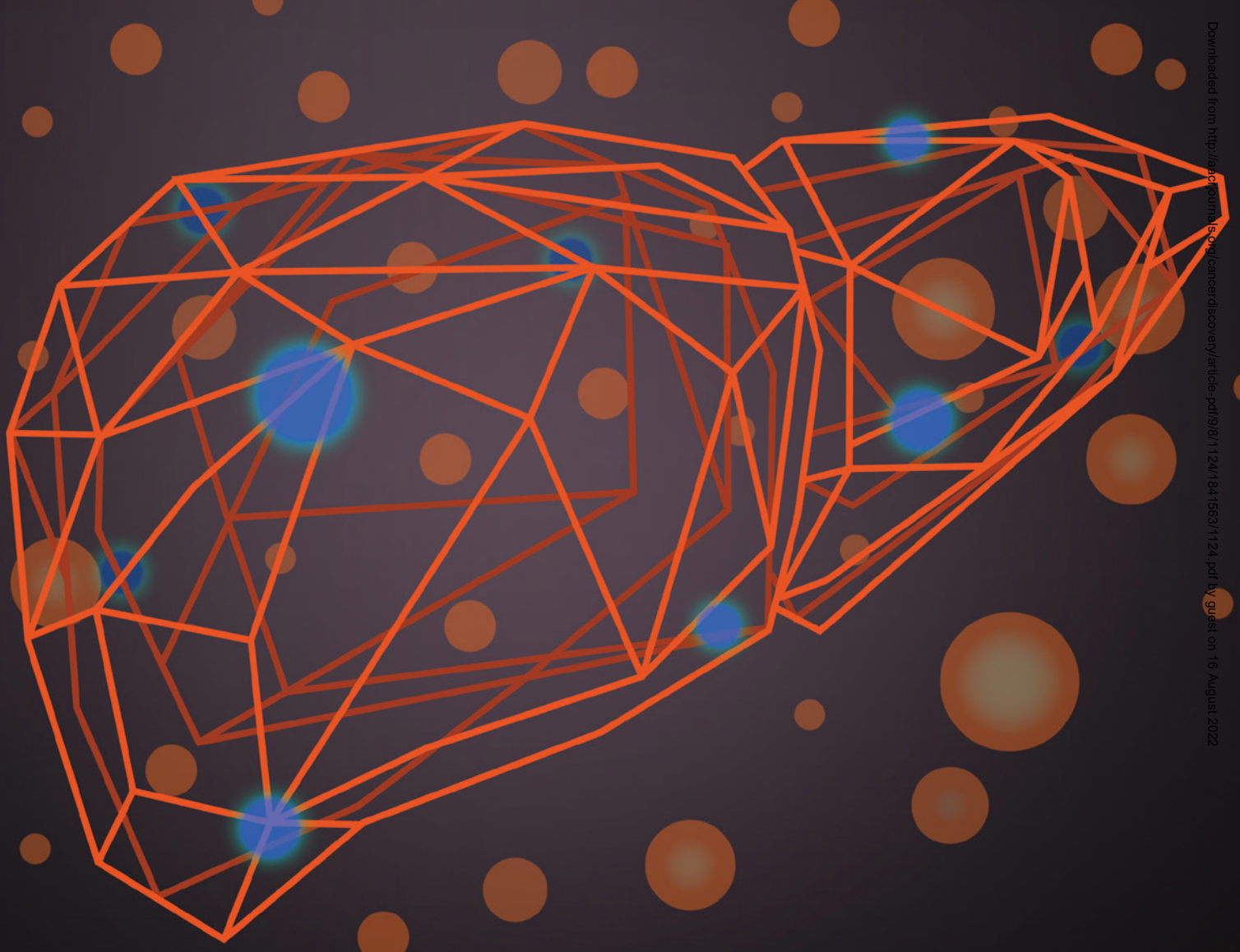

ABSTRACT PD-1 immune checkpoint inhibitors have produced encouraging results in patients with hepatocellular carcinoma (HCC). However, what determines resistance to anti–PD-1 therapies is unclear. We created a novel genetically engineered mouse model of HCC that enables interrogation of how different genetic alterations affect immune surveillance and response to immunotherapies. Expression of exogenous antigens in *MYC;Trp53*$^{-/-}$ HCCs led to T cell–mediated immune surveillance, which was accompanied by decreased tumor formation and increased survival. Some antigen-expressing *MYC;Trp53*$^{-/-}$ HCCs escaped the immune system by upregulating the β-catenin (CTNNB1) pathway. Accordingly, expression of exogenous antigens in *MYC;CTNNB1* HCCs had no effect, demonstrating that β-catenin promoted immune escape, which involved defective recruitment of dendritic cells and consequently impaired T-cell activity. Expression of chemokine CCL5 in antigen-expressing *MYC;CTNNB1* HCCs restored immune surveillance. Finally, β-catenin–driven tumors were resistant to anti–PD-1. In summary, β-catenin activation promotes immune escape and resistance to anti–PD-1 and could represent a novel biomarker for HCC patient exclusion.

SIGNIFICANCE: Determinants of response to anti–PD-1 immunotherapies in HCC are poorly understood. Using a novel mouse model of HCC, we show that β-catenin activation promotes immune evasion and resistance to anti–PD-1 therapy and could potentially represent a novel biomarker for HCC patient exclusion.

See related commentary by Berraondo et al., p. 1003.

INTRODUCTION

Hepatocellular carcinoma (HCC) represents a major health problem, causing more than 700,000 deaths annually worldwide (1). Although HCC treatment has greatly improved over the last decades, patients with HCC diagnosed at advanced stages are ineligible for curative ablative therapies such as liver resection or transplantation. Until recently, the only FDA-approved therapy for such patients was sorafenib (2), a multikinase inhibitor that provides a 3-month survival benefit on average. In the last two years, several other multikinase inhibitors have shown efficacy in patients with advanced HCC (3–5). Lenvatinib has been approved as a first-line therapy (3), and regorafenib, an inhibitor closely related to sorafenib, is approved in second line (4). Unfortunately, these multikinase inhibitors also confer limited survival benefits. More recently, nivolumab and pembrolizumab, two PD-1 immune checkpoint inhibitors, were granted accelerated approval by the FDA for HCC treatment in second line after obtaining promising outcomes in phase II clinical trials (6, 7). The results from the nivolumab and pembrolizumab trials showed that some patients with HCC achieve unprecedented responses (6, 7). However, not all patients are sensitive, indicating the existence of mechanisms that drive resistance to anti–PD-1 therapy and highlighting the urgent need to identify biomarkers for optimal patient selection.

Cancer immunotherapy is revolutionizing the clinical management of a variety of cancers (8). Among the different immunotherapy strategies, PD-1 pathway inhibitors have provided the best clinical outcomes (9–11). Unfortunately, the clinical efficacy of PD-1 pathway inhibition as monotherapy is limited to subsets of patients, with overall response rates of 20% or less (9). In other malignancies, response rates have been significantly improved through selection of patients presenting mismatch repair deficiency (12, 13) or the combination of PD-1 pathway inhibition with other therapeutic strategies, such as CTLA4 mAbs (10), strongly supporting efforts to identify biomarkers for patient selection and novel combinatorial therapies. The general consensus is that anti–PD-1 therapies are effective in tumors that are able to trigger some level of antitumor immunity, as evidenced by the existence of CD8$^+$ T-cell infiltrates (9). Conversely, most tumors that disrupt

[1]Department of Oncological Sciences, Icahn School of Medicine at Mount Sinai, New York, New York. [2]Liver Cancer Program, Division of Liver Diseases, Department of Medicine, Tisch Cancer Institute, Icahn School of Medicine at Mount Sinai, New York, New York. [3]The Precision Immunology Institute, Icahn School of Medicine at Mount Sinai, New York, New York. [4]Graduate School of Biomedical Sciences at Icahn School of Medicine at Mount Sinai, New York, New York. [5]Hospital del Mar, IMIM, Universitat Autònoma de Barcelona, Barcelona, Spain. [6]Division of Experimental Pathology, Department of Pathology, Division of Gastroenterology, Hepatology and Nutrition, Department of Medicine, University of Pittsburgh School of Medicine, Pittsburgh, Pennsylvania. [7]Pittsburgh Liver Research Center, University of Pittsburgh Medical Center and University of Pittsburgh School of Medicine, Pittsburgh, Pennsylvania. [8]First Department of Internal Medicine, University Medical Center Hamburg-Eppendorf, Hamburg, Germany. [9]Liver Cancer Translational Research Laboratory, Barcelona Clinic Liver Cancer (BCLC) Group, Liver Unit and Pathology Department, IDIBAPS, Hospital Clínic, CIBERehd, Universitat de Barcelona, Barcelona, Spain. [10]Institució Catalana de Recerca i Estudis Avançats (ICREA), Barcelona, Spain.

Note: Supplementary data for this article are available at Cancer Discovery Online (http://cancerdiscovery.aacrjournals.org/).

E. Bresnahan and P. Molina-Sánchez contributed equally to this work. K.E. Lindblad and B. Maier contributed equally to this work.

Corresponding Author: Amaia Lujambio, Tisch Cancer Institute, Precision Immunology Institute, Icahn School of Medicine at Mount Sinai, 1470 Madison Avenue Hess 6-111, New York, NY 10029. Phone: 212-824-9338; E-mail: amaia.lujambio@mssm.edu

Cancer Discov 2019;9:1124–41

doi: 10.1158/2159-8290.CD-19-0074

antitumor immunity lack CD8+ T-cell infiltration and tend to be resistant (9). Tumor-intrinsic properties, such as mutational load (14, 15), presentation of tumor antigens (16, 17), or specific oncogenic pathways (18, 19), can greatly influence antitumor immunity and response to anti–PD-1 therapies. In melanoma, activation of β-catenin (encoded by *CTNNB1*; ref. 19) or *PTEN* deletion (18) can lead to T-cell exclusion and resistance to anti–PD-1. In HCC, two recent studies in patients have shown that β-catenin activation correlates with T-cell exclusion (20) and resistance to anti–PD-1 therapy (21). However, the mechanistic link between β-catenin activation and immune resistance has not been provided, in part due to the relative delay of the clinical trials testing immunotherapies in HCC when compared with other malignancies [such as melanoma or non–small cell lung cancer (NSCLC)], and also due to the lack of appropriate models.

Several mouse models have been generated to gain insights into the mechanisms by which tumors may subvert immune responses, but each of these has critical limitations (22, 23). For example, transplantation of primary or cultured tumor cells is commonly used, but the ectopic introduction of fully developed tumor cells bypasses the initial steps of tumorigenesis and can lead to aberrant inflammatory responses (24, 25). Carcinogen-induced models lead to robust immune responses, but the presence of multiple and heterogeneous mutations hampers the understanding of the contribution of each mutated gene to the observed phenotypes (26). Genetically engineered mouse models (GEMM) of cancer accurately recapitulate both the genetic and histopathologic progression of human disease (27), but tumors tend to be nonimmunogenic and therefore fail to reproduce the interplay between tumor cells and the immune system that is characteristic of human tumors (23). Transgenic mouse models of cancer that develop tumors spontaneously and overexpress model antigens throughout targeted organs exist, but the widespread expression of the antigens tends to induce tolerance (28), failing to recapitulate the immune responses against human tumors. Recently, Tyler Jacks's laboratory has addressed these limitations by combining a conditional GEMM (*KrasG12D*$^{\text{Lox-Stop-Lox/+}}$;*Trp53*$^{\text{Lox-Lox}}$) with the delivery of lentiviruses that simultaneously express Cre recombinase (which recombines the *Lox* sites, allowing the expression of mutant *Kras* and deletion of *Trp53*) and exogenous antigens (17, 29). The expression of exogenous antigens in mosaic tumor cells led to tumor delay as a result of tumor immune surveillance (17, 29) and formally demonstrated cancer immunoediting *in vivo* (17). Although this strategy represents a technical and conceptual advancement from previous models, it is limited by the availability of existing conditional GEMMs.

In an effort to investigate the role that different genetic alterations have in HCC immune surveillance and response to immunotherapies, we have adopted a system to quickly induce autochthonous and mosaic liver tumors that harbor specific and customizable genetic alterations and varying levels of immunogenicity. The model is based on the hydrodynamic tail-vein delivery of genetic elements (30) to overexpress oncogenes (with transposon-based vectors), delete or mutate tumor suppressor genes (with CRISPR/Cas9 vectors), and modulate immunogenicity (with exogenous antigens) specifically in hepatocytes. This model, which is amenable to rapid genetic manipulation, is technically and conceptually innovative, as it will allow us to study how different tumor-intrinsic signaling pathways affect antitumor immunity. With this model, we have shown that β-catenin activation promotes immune escape in HCC. Mechanistically, β-catenin activation led to a defective recruitment of dendritic cells (DC) and antigen-specific T cells, and as a consequence, to an impaired antitumor immune response. Reexpression of chemokine (C-C motif) ligand 5 (CCL5), a chemokine found to be downregulated in both murine and human tumors driven by β-catenin activation, restored immune surveillance. Finally, β-catenin activation conferred resistance to anti–PD-1 therapy in our murine model. We have shown that our model can be used to identify mechanisms of immune escape and resistance to anti–PD-1 that are relevant to human disease and could provide the rationale for improved patient selection and personalized cancer immunotherapies.

RESULTS

Expression of Exogenous Antigens in Murine *MYC;Trp53*$^{-/-}$ HCCs Leads to a Delay in Tumor Development

Two of the most frequently altered genes in patients with HCC are the oncogene *MYC* (amplified in 17% of HCCs) and the tumor suppressor *TP53* (deleted or mutated in 33% of HCCs). Their alterations frequently co-occur in patients with HCC (6.5%), suggesting cooperation (Fig. 1A). We previously showed that we can generate liver tumors resembling human HCC by performing hydrodynamic tail-vein injections of a transposon vector expressing MYC (*pT3-EF1a-MYC*), a vector expressing SB13 transposase (*CMV-SB13*), which is required to integrate the transposon-based vector into the hepatocyte genomic DNA, and a CRISPR/Cas9 vector expressing a single-guide RNA (sgRNA) targeting *Trp53* (*px330-sg-p53*; ref. 31). Hydrodynamic tail-vein injections (30) allow the delivery of DNA specifically into the hepatocytes by creating an increase in blood pressure that redirects the flow of blood directly into the liver. To modulate the immunogenicity of the *MYC;Trp53*$^{-/-}$ liver tumors, we modified the transposon vector expressing MYC to also express luciferase (*MYC-luc*), which is mildly immunogenic (32), or a highly immunogenic version of luciferase (*MYC-lucOS*) that is linked to three model antigens: SIYRYYGL (SIY), SIINFEKL (SIN; OVA257-264), and OVA323-339 (Fig. 1B; ref. 29). Hydrodynamic injection of *px330-sg-p53* and *CMV-SB13* in combination with *MYC-luc* or *MYC-lucOS* into 6-week-old C57BL/6 female mice led to equivalent luciferase expression in the livers measured by bioluminescence imaging at day 6, indicating similar injection efficiency and expression levels in both groups (Fig. 1C and D). Interestingly, 25 days after the injection there was a drastic reduction in luciferase signal in *MYC-lucOS;sg-p53* mice, suggesting clearance of luciferase and antigen-expressing hepatocytes (Fig. 1C and D). Additional experiments demonstrated that the decrease in luciferase signal in *MYC-lucOS;sg-p53* mice occurred by day 13 after the injection (Supplementary Fig. S1A). Accordingly, tumor formation was markedly delayed in *MYC-lucOS;sg-p53* mice compared with *MYC-luc;sg-p53* mice and was accompanied by a significant increase in survival (Fig. 1E and F). Similar effects were observed in female and male C57BL/6 mice, indicating that the phenomenon occurs

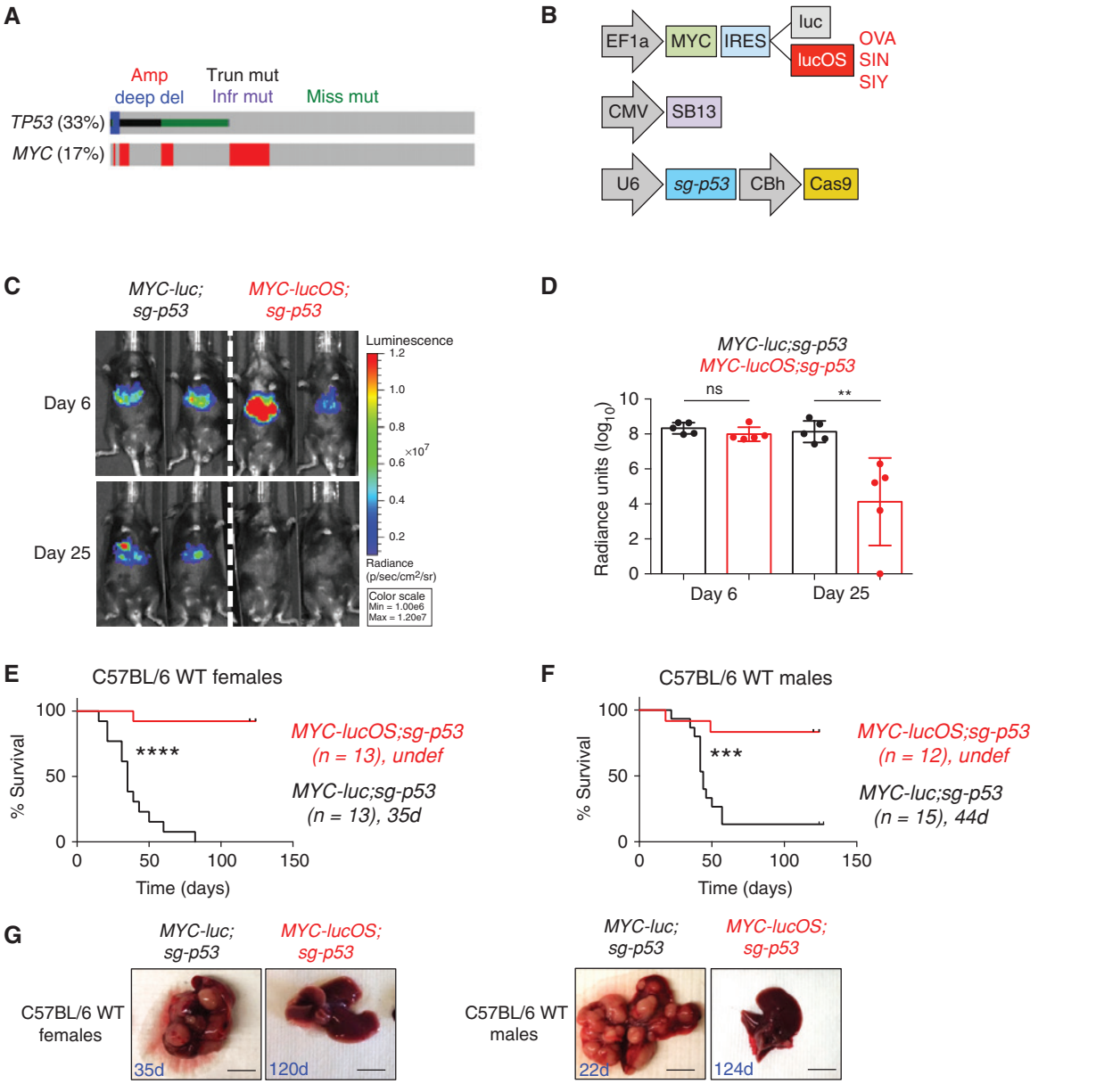

Figure 1. Expression of exogenous antigens in murine *MYC; Trp53*$^{-/-}$ HCCs leads to tumor delay. **A,** Oncoprint of *TP53* and *MYC* alterations in 366 patients with HCC (TCGA, provisional, December 2018, cBioPortal; ref. 61). The percentage of patients harboring the alteration is shown. Amp, amplification; del, deletion; trun, truncating; mut, mutation; infr, in-frame; miss, missense. **B,** Schematic of vectors injected into mice. The transposon-based vector overexpressing MYC can also express luciferase (luc) or a luciferase fused to model antigens (lucOS). **C,** Bioluminescence imaging 6 and 25 days after injection of vectors into representative mice. The color code for the luciferase signal is shown. **D,** Quantification of normalized luciferase signal 6 and 25 days after injection of vectors ($n = 5$ per group). Mean and SD are shown. Mann–Whitney test. Survival curves in C57BL/6 WT females (**E**) and males (**F**). Number of mice per group is shown as well as median survival. Undef, undefined. Log-rank Mantel–Cox test. **G,** Pictures of representative livers from **E** and **F**. The number indicates the number of days from injection to death for that particular mouse. Scale bars, 1 cm. **, $P < 0.01$; ***, $P < 0.001$; ****, $P < 0.0001$.

irrespective of sex (Fig. 1E and F). Most *MYC-lucOS;sg-p53* mice did not develop any tumors within 4 months, whereas the majority of *MYC-luc;sg-p53* mice presented gross liver tumors (Fig. 1G) that caused death, with a median survival of 35 to 44 days (Fig. 1E and F). Deep sequencing analysis of *MYC-luc;sg-p53* livers 7 days after the injection detected 5.645% frameshift mutations at the *sg-p53* target site, whereas only 0.457% indels were found in mice injected without *sg-p53*, and those indels were spread across the whole sequence, indicating background sequencing errors (Supplementary Fig. S1B and S1C). This confirms that *px330-sg-p53* can directly generate mutations in *Trp53* in the mouse liver (33). In established tumors, approximately 80% frameshift mutations and prevalence of two specific indels that produce truncated proteins were detected in tumors with *sg-p53* (Supplementary Fig. S1D and S1E), suggesting selection from a single *Trp53*-mutated cell. In addition, transgenic MYC overexpression was confirmed in *MYC;Trp53*$^{-/-}$ HCCs when compared with normal

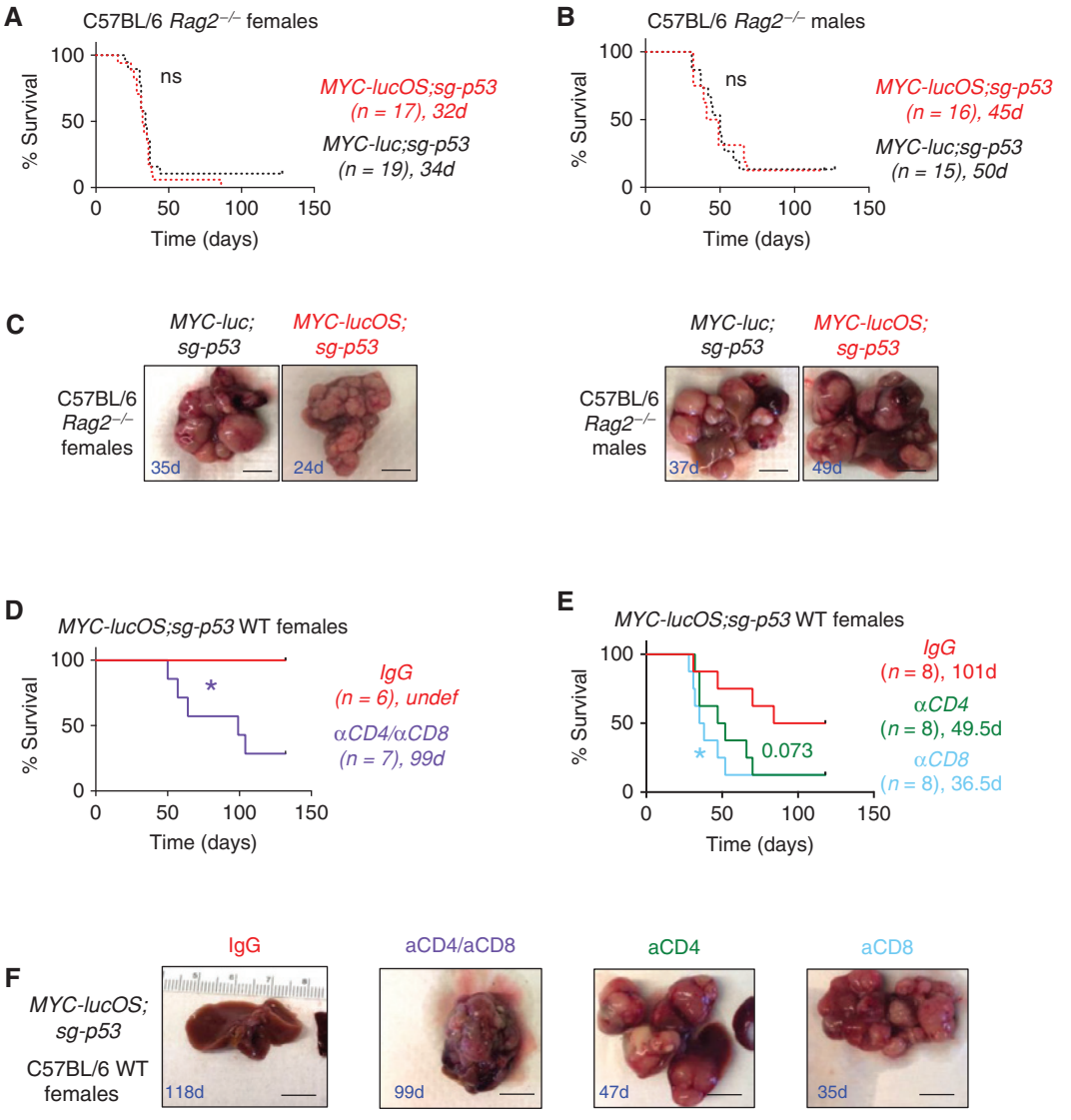

Figure 2. CD8+ T cells eliminate antigen-expressing *MYC;Trp53*$^{-/-}$ HCCs. Survival curves in C57BL/6 *Rag2*$^{-/-}$ females (**A**) and males (**B**). Number of mice per group is shown as well as median survival. Log-rank Mantel–Cox test. **C,** Pictures of representative livers from **A** and **B**. The number indicates the number of days from injection to death for that particular mouse. Scale bars, 1 cm. Survival curves in C57BL/6 WT with combined CD4+ and CD8+ T-cell depletion (**D**) or separate CD4+ and CD8+ T-cell depletion (**E**). Number of mice per group is shown as well as median survival. Undef, undefined. Log-rank Mantel–Cox test. Comparisons are to control mice injected with isotype control antibodies (IgG). **F,** Pictures of representative livers from **D** and **E**. The number indicates the number of days from injection to death for that particular mouse. Scale bars, 1 cm. *, $P < 0.05$.

livers (Supplementary Fig. S1F). Taken together, expression of exogenous antigens leads to tumor delay in the context of murine *MYC;Trp53*$^{-/-}$ HCCs.

CD8+ T Cells Eliminate Antigen-Expressing *MYC;Trp53*$^{-/-}$ HCCs

To functionally interrogate the involvement of T cells in the elimination of antigen-expressing cancer cells, we performed hydrodynamic injection of *px330-sg-p53* and *CMV-SB13* in combination with *MYC-luc* or *MYC-lucOS* into 6-week-old B and T cell–deficient *Rag2*$^{-/-}$ mice in C57BL/6 background (Fig. 2A and B; Supplementary Fig. S2A–S2D). The survival benefit observed in wild-type (WT) mice harboring *MYC-lucOS;sg-p53* tumors was abolished in *Rag2*$^{-/-}$ mice (Figs. 1E and F and 2A and B; Supplementary Fig. S2A and S2B), confirming the role of lymphocytes in eliminating antigen-expressing hepatocytes. In contrast, lack of B and T cells in *Rag2*$^{-/-}$ mice had no significant effect in the development of *MYC-luc;sg-p53* tumors (Supplementary Fig. S2C and S2D), indicating that the expression of antigens is critical for an effective lymphocyte-mediated immune response. Both *MYC-lucOS;sg-p53* and *MYC-luc;sg-p53 Rag2*$^{-/-}$ mice developed large macroscopic tumors (Fig. 2C) that caused death, with a median survival of 32 to 50 days (Fig. 2A and B; Supplementary Fig. S2A–S2D). Luciferase signal was similar between WT and immunodeficient mice three days after the

hydrodynamic injection (Supplementary Fig. S2E), ruling out that the differences observed in tumorigenesis could be due to distinct hepatocyte transfection efficiency. Moreover, injection of anti-CD4 and anti-CD8 antibodies into *MYC-lucOS;sg-p53* WT mice durably depleted $CD4^+$ and $CD8^+$ T cells (Supplementary Fig. S2F and S2G) and led to a decrease in survival when compared with mice treated with control antibodies (Fig. 2D–F), further confirming the role of T lymphocytes in eliminating antigen-expressing hepatocytes. Additional experiments demonstrated that mainly $CD8^+$ ($P = 0.0351$) but also $CD4^+$ T cells to some extent ($P = 0.0730$) were involved in the elimination of antigen-expressing *MYC;Trp53*$^{-/-}$ tumor cells (Fig. 2E and F; Supplementary Fig. S2G). Taken together, expression of exogenous antigens in the context of MYC overexpression and *Trp53* loss in murine hepatocytes leads to immune surveillance mediated primarily by $CD8^+$ T cells.

β-Catenin Signaling Is Activated in Immune-Escaped *MYC;Trp53*$^{-/-}$ HCC Tumors

The expression of antigens in the context of murine *MYC;Trp53*$^{-/-}$ HCC tumors leads to immune surveillance. However, the clearance of tumor cells was not complete in all mice, and some tumors eventually escaped the immune system (Fig. 1E and F). To identify the signaling pathways involved in the immune escape of *MYC-lucOS;sg-p53* tumors, we performed RNA sequencing (RNA-seq) of bulk tumors from *MYC-luc;sg-p53* and *MYC-lucOS;sg-p53* female mice. Gene set enrichment analysis (GSEA; ref. 34) was used to evaluate functional enrichment of datasets related to different signaling pathways involved in HCC. Analysis of 188 oncogenic signatures available at MSigDB Collections (35) showed no significant differences between the two groups (Supplementary Table S1). Analysis of four HCC-specific gene signatures (36) demonstrated that a molecular class associated with *CTNNB1* (β-catenin)-mutant human HCCs was significantly enriched in escaped *MYC-lucOS;sg-p53* tumors (Fig. 3A; Supplementary Fig. S3A). Indeed, although the general transcriptional differences were minimal, *Axin2*, a direct target of β-catenin, was one of the top overexpressed genes in escaped *MYC-lucOS;sg-p53* tumors (Fig. 3B), suggesting that β-catenin activation may be involved in immune escape in HCC. *Axin2* overexpression was confirmed in a larger set of *MYC-luc;sg-p53* and escaped *MYC-lucOS;sg-p53* tumors by qRT-PCR (Fig. 3C) and also by protein analysis (Supplementary Fig. S3B). Only one out of 22 *MYC-luc;sg-p53* tumors presented *Axin2* mRNA levels that were higher than the mean expression in escaped *MYC-lucOS;sg-p53* tumors, whereas eight out of 23 *MYC-lucOS;sg-p53* tumors had *Axin2* levels higher than the mean (Fig. 3D).

To better understand mechanisms of immune escape in HCC, we performed RNA-seq of four additional escaped *MYC-lucOS;sg-p53* tumors with low levels of *Axin2* (hereafter referred to as low-*Axin2*–escaped tumors), which suggests they escaped through a different immune escape mechanism, and compared them to the escaped *MYC-lucOS;sg-p53* tumors analyzed before (hereafter referred to as *Axin2*-escaped tumors; Fig. 3A and B). As expected, the molecular class associated with *CTNNB1* (β-catenin)-mutant human HCCs (36) was enriched in *Axin2*-escaped tumors (Fig. 3E). Interestingly, a gene set related to adaptive immune response was significantly enriched in low-*Axin2*–escaped tumors (Fig. 3F), suggesting that there may be an association between β-catenin activation and the type of immune escape mechanism. *CTNNB1* mRNA levels were unchanged (Supplementary Fig. S3C), which suggests that β-catenin activation, rather than *CTNNB1* mRNA levels, is critical for its activity. To test whether β-catenin activation occurred in tumor cells, we separated tumor cells from immune cells in escaped *MYC-lucOS;sgp53* tumors by Percoll gradient centrifugation. *Axin2* was found predominantly overexpressed in tumor cells in the escaped *MYC-lucOS;sg-p53* tumors (Supplementary Fig. S3D). However, because stromal cells could not be separated from the bulk hepatocyte fraction, we cannot rule out that stromal cells may contribute to the increase in *Axin2* levels and activation of the β-catenin pathway seen in *MYC-lucOS;sg-p53* tumors. Interestingly, β-catenin activation promotes immune escape and resistance to anti–PD-1 therapy in melanoma (19) and correlates with "non-T cell–inflamed" HCC tumors (20) and resistance to anti–PD-1 therapy in patients with HCC (21), which together with our data suggests a role for β-catenin activation in HCC immune escape in a subset of HCC tumors.

β-Catenin Signaling Activation Promotes Immune Escape in HCC

CTNNB1 is frequently altered in patients with HCC (mutated in 27% to 37% of HCCs; refs. 37, 38), together with *MYC* amplification (Fig. 4A). To address whether or not β-catenin activation in tumor cells could promote immune escape of HCCs, we tested the effects of the expression of exogenous antigens in the context of β-catenin activation. For that, we performed hydrodynamic tail-vein injections of a transposon vector expressing activated β-catenin (*CTNNB1-N90*, which presents a deletion of the first 90 amino acids leading to constitutive activation; ref. 39) in combination with *MYC-luc* or *MYC-lucOS* and *CMV-SB13* into 6-week-old C57BL/6 female mice (Fig. 4B). Luciferase signal, measured by bioluminescence imaging, in the livers at day six was similar in the two groups (significantly lower in *MYC-lucOS;CTNNB1* mice although within the same order of magnitude), indicating similar injection efficiency and expression levels (Fig. 4C and D). However, contrary to *MYC-lucOS;sg-p53* mice, which showed a drastic reduction in luciferase signal at 25 days (Fig. 1C and D), *MYC-lucOS;CTNNB1* mice showed strong luciferase signal at 27 days, indicating the presence of antigen-expressing hepatocytes and the absence of tumor cell clearance (Fig. 4C and D). Accordingly, tumor formation and survival were similar in *MYC-lucOS;CTNNB1* and *MYC-luc;CTNNB1* mice (Fig. 4E–G), suggesting that activated β-catenin impairs immune surveillance and promotes immune escape. Similar effects were observed in female and male C57BL/6 mice, indicating that the phenotype is not affected by sex (Fig. 4E–G). Both *MYC-lucOS;CTNNB1* and *MYC-luc;CTNNB1* mice developed large macroscopic tumors (Fig. 4G) that caused death with a median survival of 35 to 48 days (Fig. 2E–G), a latency comparable with *MYC-luc;sg-p53* mice. As expected, absence of B and T cells in *Rag2*$^{-/-}$ mice had no significant impact in the tumor growth of *MYC-luc;CTNNB1* and *MYC-lucOS;CTNNB1* tumors (Supplementary Fig. S4A–S4C), further demonstrating

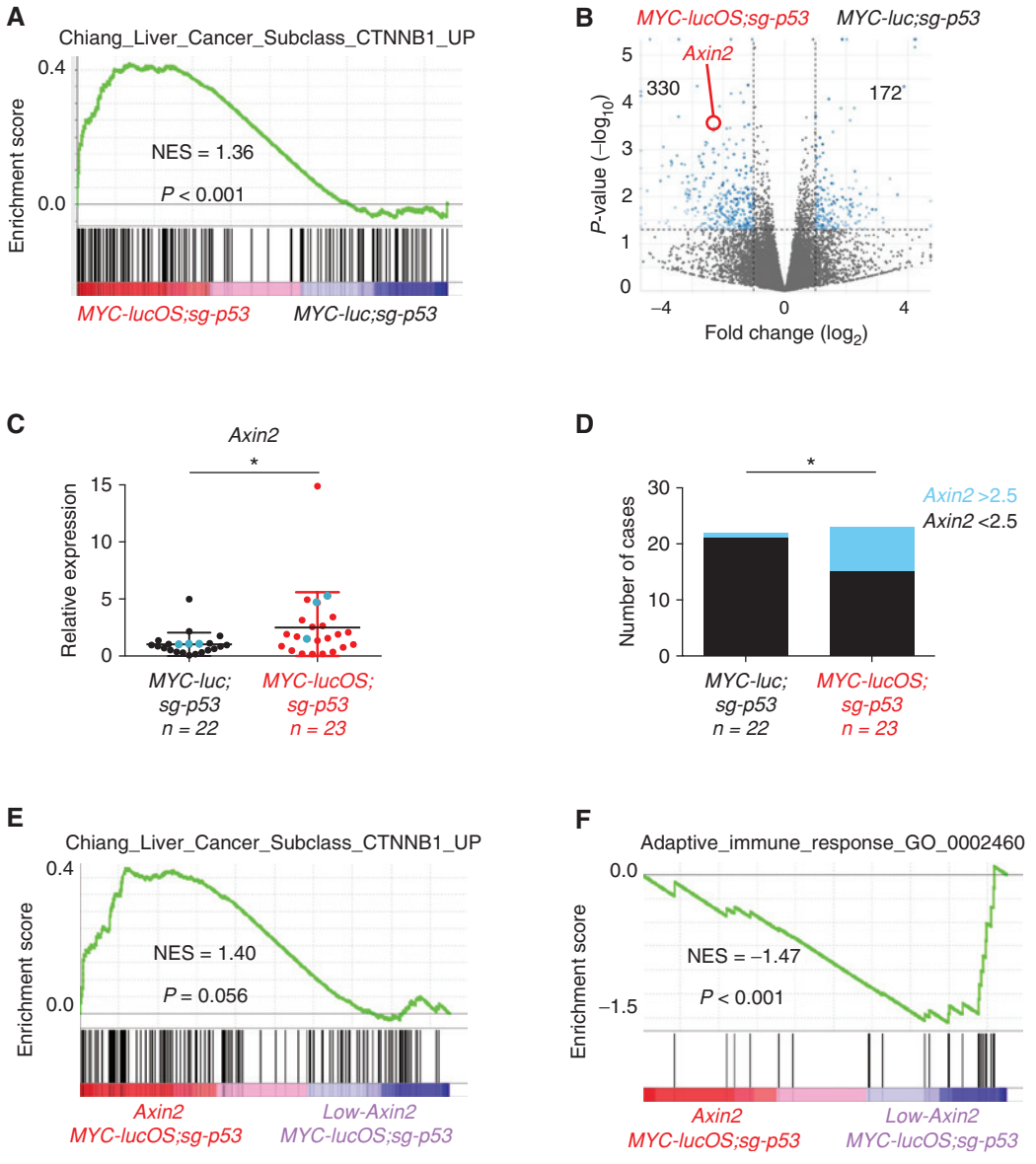

Figure 3. β-catenin signaling is activated in immune-escaped HCC tumors. **A,** GSEA of an HCC *CTNNB1* gene signature in escaped *MYC-lucOS;sg-p53* tumors ($n = 3$ per group). NES, normalized enrichment score. **B,** Volcano plot representing genes according to their fold change and *P* value in *MYC-luc;sg-p53* escaped tumors when compared with *MYC-lucOS;sg-p53* tumors. *Axin2* is highlighted in red. **C,** Relative levels of *Axin2* in *MYC-luc;sg-p53* and escaped *MYC-lucOS;sg-p53* tumors by qRT-PCR. Each dot represents one tumor coming from one independent mouse. Number of samples is shown. The samples used in the RNA-seq (**A** and **B**) are highlighted in blue. Mean and SD are shown. Mann–Whitney test. **D,** Number of cases with *Axin2* levels higher (blue) or lower (black) than 2.5 (which is the mean value in *MYC-lucOS;sg-p53* tumors in **C**). Number of samples is shown. Fisher exact test. GSEA of an HCC *CTNNB1* gene signature (**E**) and an adaptive immune response signature (**F**) in *Axin2*-escaped *MYC-lucOS;sg-p53* tumors ($n = 3$) or low-*Axin2*–escaped *MYC-lucOS;sg-p53* tumors ($n = 4$). *, $P < 0.05$.

that antigen expression in the context of MYC overexpression and β-catenin activation does not lead to immune surveillance and β-catenin activation promotes immune escape.

Luciferase signal was equivalent in *MYC-luc;sg-p53, MYC-lucOS;sg-p53, MYC-luc;CTNNB1*, and *MYC-lucOS;CTNNB1* livers six days after the hydrodynamic injection (Supplementary Fig. S4D), excluding that differences in initial hepatocyte transfection could have an effect on the immune surveillance and immune escape observed in the *MYC-lucOS;sg-p53* and *MYC-lucOS;CTNNB1* mice, respectively. Furthermore, *MYC-luc;sg-p53* and *MYC-luc;CTNNB1* mice, which are not subjected to immune pressure, presented similar median survival [35 vs. 35.5 days in females (Figs. 1E and 4E); 44 vs. 42 days in males (Figs. 1F and 4F)], indicating that the tumor growth rate was similar in both models. As expected, *MYC;CTNNB1* tumors overexpressed MYC, activated β-catenin, and displayed WT p53 (Supplementary Figs. S1E and S4E). To address whether β-catenin activation is truly driving immune escape of *MYC-lucOS;CTNNB1* tumors and to rule out the

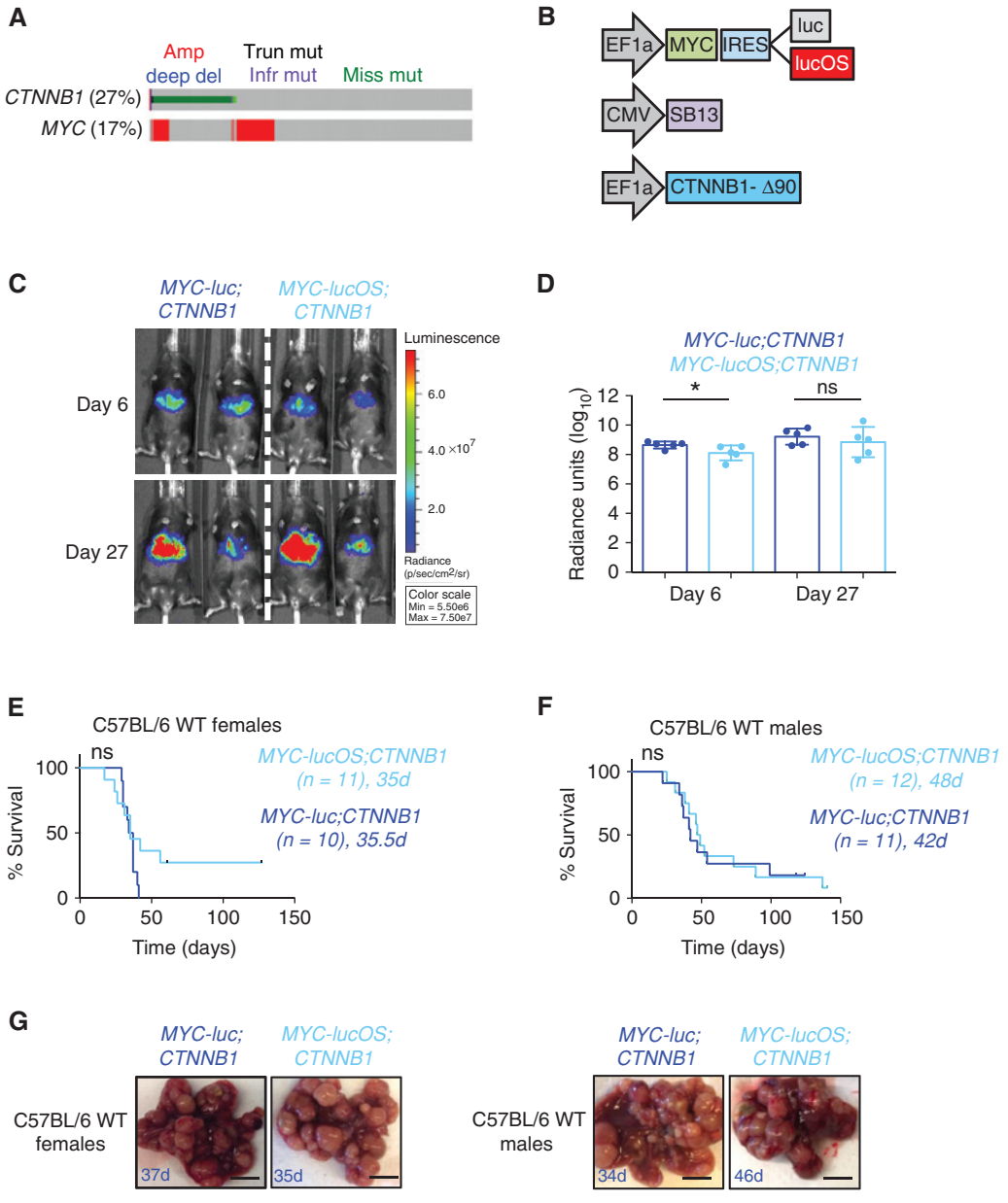

Figure 4. β-catenin signaling activation promotes immune escape in HCC. **A,** Oncoprint of *CTNNB1* and *MYC* alterations in 366 patients with HCC (TCGA, provisional, December 2018, cBioPortal; ref. 61). The percentage of patients harboring the alteration is shown. Amp, amplification; del, deletion; trun, truncating; mut, mutation; infr, in-frame; miss, missense. **B,** Schematic of vectors injected into mice. The transposon-based vector overexpressing MYC can also express luciferase (luc) or a luciferase fused to model antigens (lucOS). **C,** Bioluminescence imaging 6 and 27 days after injection of vectors into representative mice. The color code for the luciferase signal is shown. **D,** Quantification of normalized luciferase signal 6 and 27 days after injection of vectors ($n = 5$ per group). Mean and SD are shown. Mann–Whitney test. Survival curves in C57BL/6 WT females (**E**) and males (**F**). Number of mice per group is shown as well as median survival. Log-rank Mantel–Cox test. **G,** Pictures of representative livers from **E** and **F**. The number indicates the number of days from injection to death for that particular mouse. Scale bars, 1 cm. *, $P < 0.05$.

potential involvement of WT p53, we assessed the effect of mutating p53 in the context of *MYC-lucOS;CTNNB1* tumors. Tumor formation and survival were equivalent in *MYC-lucOS;CTNNB1;sg-p53* and *MYC-lucOS;CTNNB1* mice (Supplementary Fig. S4F and S4G), confirming the role of β-catenin activation in driving immune escape of *MYC-lucOS;CTNNB1* tumors. These results also indicate that β-catenin activation can directly promote immune escape of *MYC-lucOS; sg-p53* tumors, which otherwise undergo immune surveillance (Fig. 1).

β-Catenin Activation Impairs DC Recruitment in the Context of HCC

There are multiple mechanisms by which cancer cells escape the immune system, involving changes in cancer and/or immune cells (8). To identify the potential changes in cancer

cells contributing to β-catenin activation–mediated immune escape, we performed RNA-seq of bulk tumors from *MYC-luc;CTNNB1* and *MYC-lucOS;CTNNB1* female mice. As expected, β-catenin–driven tumors were significantly enriched in the dataset representing *CTNNB1*-mutant human HCCs (36) when compared with *MYC-luc;sg-p53* tumors (Supplementary Table S2). In addition, levels of *Axin2,* a direct target of β-catenin, were higher in the β-catenin–driven tumors when compared with *MYC-luc;sg-p53* tumors by qRT-PCR in a larger subset of tumors (Supplementary Fig. S5A). Moreover, luciferase transcripts were present in both groups, at similar levels, whereas transcripts corresponding to the OS region of *lucOS* were present in only *MYC-lucOS;CTNNB1* tumors, confirming that antigen expression was not lost in the immune-escaped tumors (Supplementary Fig. S5B). High PD-L1 (CD274) has been observed in metastatic *CTNNB1*-mutant HCC tumor cells (40). In our murine tumors, *Pdl1* expression was similar in *MYC-luc;sg-p53* and β-catenin–driven tumor cells (Supplementary Fig. S5C), suggesting that the immune escape observed in β-catenin–driven tumors was not due to *Pdl1* expression in tumor cells. Interestingly, transcriptional differences between *MYC-luc;CTNNB1* and *MYC-lucOS;CTNNB1* tumors were negligible (156 genes overexpressed and 183 genes downregulated in *MYC-lucOS;CTNNB1* tumors compared with *MYC-luc;CTNNB1* tumors). The lack of changes in the "lucOS-expressing" tumors suggested that *MYC-lucOS;CTNNB1* tumors may not be subjected to immune pressure, unlike *MYC-lucOS;sg-p53* tumors, and that β-catenin could drive a program that completely abolishes the antitumor immune response.

To identify mechanisms of immune escape related to changes in the immune cell compartment, we performed flow cytometry analysis of the livers two weeks after the injections, a time point that already shows a decrease in luciferase signal (Supplementary Fig. S1A), in control WT, *MYC-lucOS;sg-p53*, and *MYC-lucOS;CTNNB1* mice. The *lucOS* transgene leads to the expression of the model antigens SIYRYYGL (SIY), SIINFEKL (SIN; OVA257-264), and OVA323-339 (Fig. 1B; ref. 29). SIINFEKL-specific $CD8^+$ T cells were significantly more abundant in *MYC-lucOS;sg-p53* livers when compared with *MYC-lucOS;CTNNB1* or healthy livers (Fig. 5A). To prime antigen-specific $CD8^+$ T cells, DCs are required. DC1 cells (DAP $I^-CD45^+lin^-MHCII^+CD11c^+CD24^+CD103^+CD11b^-$) were significantly more abundant in *MYC-lucOS;sg-p53* livers when compared with *MYC-lucOS;CTNNB1* or healthy livers (Fig. 5B), although DC1 presence was comparable in the spleens (Supplementary Fig. S5D). There were no significant differences in the total numbers of $CD8^+$ T cells, $CD4^+$ T cells, natural killer (NK) cells ($DAPI^-CD45^+lin^-NK1.1^+$), Kupffer cells (KC; $DAPI^-CD45^+Ly6G^-CD11c^{lo}CD11b^+F4/80^{hi}$), monocyte-derived macrophages ($DAPI^-CD45^+Ly6G^-CD11c^+CD11b^{hi}F4/80^{int}Ly6C^{-/lo}$), DC2 ($DAPI^-CD45^+lin^-MHCII^+CD11c^+CD24^+CD103^-CD11b^+$), or monocytes ($DAPI^-CD45^+Ly6G^-CD11c^+CD11b^{hi}F4/80^{int}Ly6C^{hi}$) between *MYC-lucOS;sg-p53* and *MYC-lucOS;CTNNB1* livers (Supplementary Fig. S5E). The percentage of neutrophils ($DAPI^-CD45^+Lin^-CD11b^+Ly6C^{lo}Ly6G^+$) was also unchanged (Supplementary Fig. S5F). Interestingly, the increase in antigen-specific $CD8^+$ T cells was not observed on 7, 14, or 21 days after the injection in *MYC-luc;sg-p53* livers, as expected, but was found in *MYC-lucOS;sg-p53* livers at 14 and 21 days (Supplementary Fig. S5G). However, antigen-specific $CD8^+$ T cells were not found in blood at the same time points (Supplementary Fig. S5H). To functionally interrogate the involvement of DCs in an effective antitumor immune response in mice harboring HCCs, we performed hydrodynamic injection of *px330-sg-p53* and *CMV-SB13* in combination with *MYC-lucOS* into 6-week-old *Batf3*$^{-/-}$ female mice, which lack $CD103^+$ DCs (ref. 41; Fig. 5C and D). Absence of DCs in *Batf3*$^{-/-}$ mice abolished the survival benefit observed in WT mice harboring *MYC-lucOS;sg-p53* tumors (Fig. 5C and D). Moreover, DC1 and antigen-specific $CD8^+$ T cells were absent in *MYC-lucOS;sg-p53 Batf3*$^{-/-}$ livers (Fig. 5E and F), demonstrating that DCs are critical in the priming of antigen-specific $CD8^+$ T cells.

To test whether escaped *MYC-lucOS;sg-p53* tumors also present reduced numbers of DC1 and antigen-specific $CD8^+$ T cells, we performed flow cytometry in escaped *MYC-lucOS;sg-p53* established tumors and found that the presence of DC1 cells was similar to normal livers whereas antigen-specific $CD8^+$ T cells were significantly higher (Supplementary Fig. S5I and S5J), although not to the same level as after two weeks (Fig. 5A). Given that β-catenin activation was significantly lower in *Axin2*-escaped *MYC-lucOS;sg-p53* tumors compared with *MYC;CTNNB1* tumors (Fig. 5G; Supplementary Table S3), we reasoned that *Axin2*-escaped *MYC-lucOS;sg-p53* tumors may present an intermediate level of activation of β-catenin and therefore undergo an immune escape that is also phenotypically intermediate. In fact, transcripts related to DCs, such as *Batf3, Itgae* (*Cd103*), *Irf8*, and *Thbd* (*Cd141*), and to T cells, including *Cd3d, Cd3e, Cd4, Cd8a*, and *Cd8b1*, in general displayed intermediate levels compared with *MYC-luc;sg-p53* (without immune pressure) and low-*Axin2*–escaped *MYC-lucOS;sg-p53* tumors, which present abundant immune transcripts (Fig. 5G; Supplementary Table S3). *MYC-lucOS;CTNNB1* tumors, with high activation of the β-catenin pathway, harbored significantly less immune-related transcripts, suggesting that they are immune-excluded (Fig. 5G; Supplementary Table S3). Similar results were obtained by immunofluorescence staining for the T-cell marker CD3 in *MYC-lucOS;sg-p53* and *MYC-lucOS;CTNNB1* livers at 2 weeks, recapitulating the flow cytometry results (Supplementary Fig. S5E and S5K), and, in established tumors, recapitulating the RNA-seq results (Fig. 5G; Supplementary Fig. S5K).

We also assessed the transcriptional profiles of 360 samples from patients with HCC [liver hepatocellular carcinoma (LIHC), available at The Cancer Genome Atlas (TCGA); ref. 37]. As expected, *CTNNB1*-mutant samples (97/360, 26.79%) were significantly enriched in the dataset representing *CTNNB1*-mutant HCCs (36) when compared with *CTNNB1* WT samples (Supplementary Table S2). In fact, expression of *AXIN2* and *GLUL*, two well-established targets of β-catenin, was significantly higher in *CTNNB1*-mutant samples (Fig. 5H; Supplementary Table S4). Most importantly, *CTNNB1*-mutant samples presented significantly reduced expression of DC markers (*BATF3, IRF8, THBD*), T-cell markers (*CD3D, CD3E, CD4, CD8A*), and the exhaustion marker *PDCD1* (PD-1; Fig. 5H; Supplementary Table S3), suggesting that *CTNNB1*-mutant HCCs exhibit immune exclusion. In fact, in a cohort of 59 HCC patient samples, nuclear staining of β-catenin was associated with significantly lower numbers of $CD8^+$ T cells in the tumors (Fig. 5I and J), and in another cohort of 216

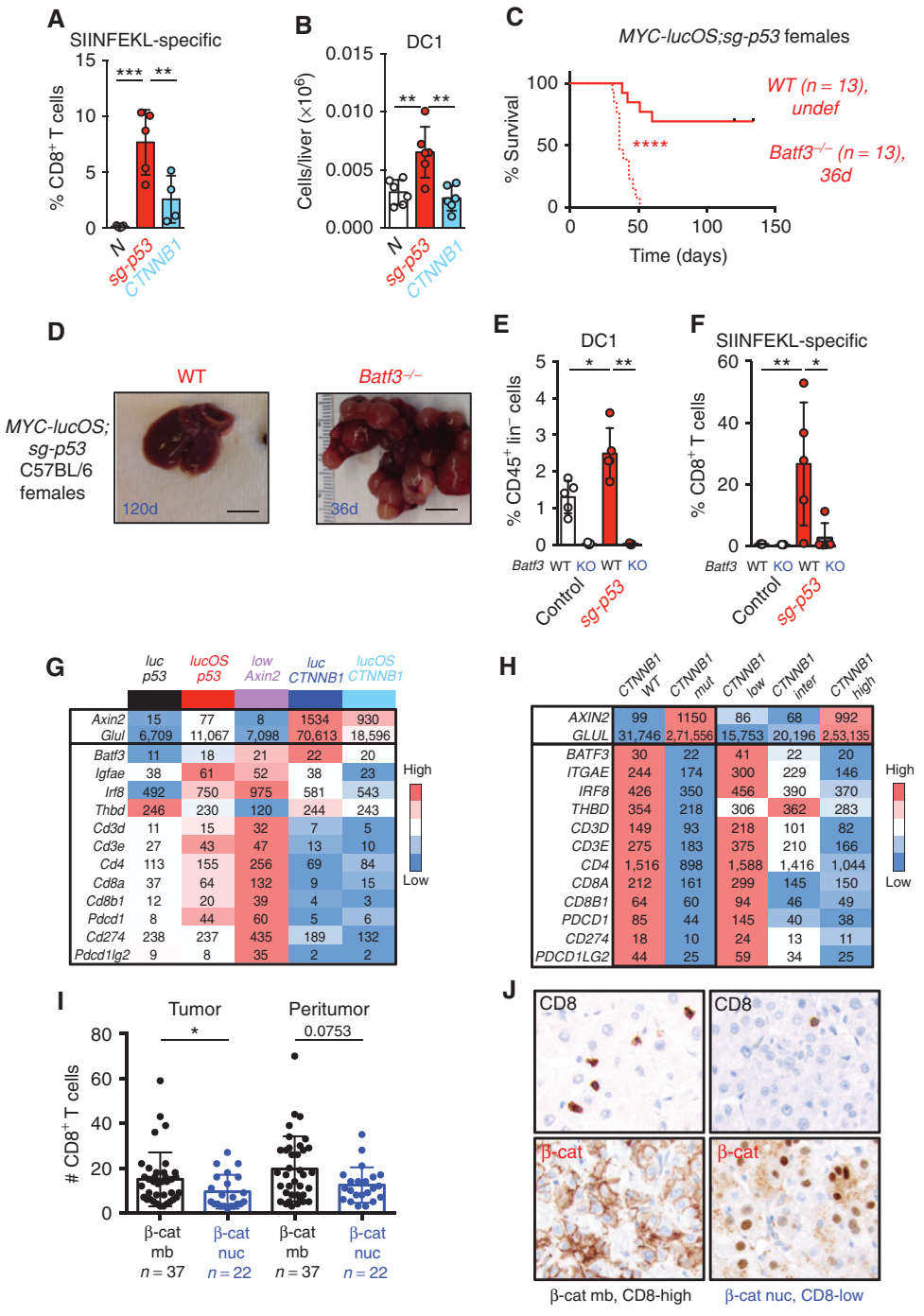

Figure 5. β-catenin impairs DC recruitment in the context of HCC. Quantification of the percentage of SIINFEKL-specific CD8+ T cells (**A**) or number of DC1 DCs (**B**) in the livers of the corresponding mice ($n = 5$–6 per group). Representative of three independent experiments. N, normal liver; *sg-p53, MYC-lucOS;sg-p53*; *CTNNB1, MYC-lucOS;CTNNB1*. Mean and SD are shown. ANOVA test. **C,** Survival curves in C57BL/6 WT or *Batf3*$^{-/-}$ females harboring *MYC-lucOS;sg-p53* tumors. *Batf3*$^{-/-}$ mice are represented with a dotted line. Number of mice per group is shown as well as median survival. Undef, undefined. Log-rank Mantel–Cox test. **D,** Pictures of representative livers from **C**. The number indicates the number of days from injection to death for that particular mouse. Scale bars, 1 cm. Quantification of the number of DC1 dendritic cells (**E**) or the percentage of SIINFEKL-specific CD8+ T cells (**F**) in the livers of the corresponding mice ($n = 5$ per group). *sg-p53, MYC-lucOS;sg-p53*; Control, noninjected; KO, *Batf3*$^{-/-}$. Mean and SD are shown. ANOVA test. Heat map showing the average expression values of different genes in murine tumors (**G**) and human TCGA tumors (**H**). Colors are adjusted for each row and for each group comparison from high (red) to low (blue). *luc p53, MYC-luc;sg-p53* ($n = 3$); *lucOS p53, MYC-lucOS;sg-p53* ($n = 3$); low *Axin2*, low-*Axin2*–escaped *MYC-lucOS;sg-p53* ($n = 4$); luc *CTNNB1, MYC-luc;CTNNB1* ($n = 7$); *lucOS CTNNB1, MYC-lucOS;CTNNB1* ($n = 5$); *CTNNB1* WT, wild-type ($n = 263$); *CTNNB1* mut, mutant ($n = 97$); CTNNB1 low ($n = 120$); CTNNB1 inter, intermediate ($n = 120$); CTNNB1 high ($n = 120$). Samples were stratified depending on *CTNNB1* status as WT or mutant, or *CTNNB1*-mutant HCC gene signature enrichment levels (in tertiles). **I,** Number of CD8+ T cells in tumor and peritumor areas in HCC patient samples ($n = 59$), which were classified as having membrane (mb; $n = 37$) or nuclear (nuc; $n = 22$) staining for β-catenin protein. Mean and SD are shown. Mann–Whitney test. **J,** Representative pictures of the stainings for CD8 and β-catenin summarized in **I**. *, $P < 0.05$; **, $P < 0.01$; ***, $P < 0.001$; ****, $P < 0.0001$.

patients with HCC, those with enrichment of *CTNNB1*-mutant HCC signature (36) were associated with a significant decrease in immune cell infiltration assessed by hematoxylin and eosin staining (Supplementary Fig. S5L). To test the importance of β-catenin pathway activation levels on the immune escape phenotype, we stratified the 360 patients with HCC according to their level of enrichment of the dataset representing *CTNNB1*-mutant HCCs (ref. 36; low, first tertile; intermediate, second tertile; high, third tertile). As observed in the murine tumors (Fig. 5G; Supplementary Table S3), samples from patients with HCC with intermediate and high activation of the β-catenin pathway presented less immune cell transcripts than samples in the low activation group, further suggesting that β-catenin pathway activation levels have an impact on the extent of immune exclusion. Taken together, the immune escape driven by β-catenin activation is mediated by a defect in DC recruitment, which in turn impairs the subsequent antitumor immune response, in both murine and human HCCs.

CCL5 Expression Restores Immune Surveillance in β-Catenin–Driven HCCs

To identify mechanisms explaining the defective DC activity in the context of β-catenin activation in HCC, we explored the expression of chemokines in *MYC-luc;sg-p53* tumors (control; not exposed to immune pressure) and β-catenin–driven tumors (*MYC-lucOS;CTNNB1* and *MYC-luc;CTNNB1*). Six chemokines (CCL5, CXCL1, CCL20, CCL28, CCL17, and CXCL10) out of 34 chemokines quantified by RNA-seq were significantly downregulated in β-catenin–driven tumors (there were no chemokines upregulated; Fig. 6A; Supplementary Fig. S6A; Supplementary Table S5). Among these, CCL5, CCL20, and CXCL1 were also downregulated in human *CTNNB1*-mutant HCC samples (Supplementary Fig. S6B; Supplementary Table S6). Because CCL5 has been shown to affect different immune cells, including DCs (42), we decided to focus on CCL5. We further confirmed the low levels of *Ccl5* in murine β-catenin–driven tumors by qRT-PCR of an independent subset of *MYC-luc;sg-p53* tumors (control; not exposed to immune pressure) and β-catenin–driven tumors (*MYC-lucOS;CTNNB1* and *MYC-luc;CTNNB1*; Supplementary Fig. S6C). *Ccl5* levels were similar in *MYC-luc;sg-p53* and *Axin2*-escaped *MYC-lucOS;sg-p53* tumors. However, compared with low-*Axin2*–escaped *MYC-lucOS;sg-p53* tumors, *Ccl5* levels were slightly lower (although not statistically significant) in *Axin2*-escaped *MYC-lucOS;sg-p53* tumors (Supplementary Fig. S6D), which present intermediate activation of the β-catenin pathway (Fig. 5G). Similarly, in TCGA HCC patient samples, there was a graded decrease in *CCL5* expression with increasing β-catenin activation: Tumors with the lowest activation of the β-catenin pathway showed higher *CCL5* expression than tumors with intermediate activation of the β-catenin pathway (although again not statistically significant; Fig. 6B). However, tumors with high activation of the β-catenin pathway displayed significantly less *CCL5* than tumors with low activation of β-catenin, further supporting the link between β-catenin and *CCL5* expression (Fig. 6B). *Ccl5* was found to be expressed in both immune and tumor cells in *MYC-luc;sg-p53* mice (Supplementary Fig. S6E). Interestingly, *Ccl5* expression increased significantly in *MYC-lucOS;sg-p53* livers between 7 and 21 days (Supplementary Fig. S6F), replicating the timing of immune cell infiltration and suggesting that CCL5 may be a critical mediator of the antitumor immune response.

To test whether or not CCL5 overexpression in tumor cells could somehow elicit an antitumor immune response and revert the immune escape observed in β-catenin–driven tumors, we tested the effects of the expression of model antigens in the context of simultaneous β-catenin activation and CCL5 overexpression. For that, we cloned a cDNA encoding for *Ccl5* in the same vector as *CTNNB1-N90* (Fig. 6C). We then performed hydrodynamic tail-vein injections of this vector in combination with *MYC-luc* or *MYC-lucOS* and *CMV-SB13* into 6-week-old C57BL/6 female mice. Tumor formation and survival were significantly delayed in *MYC-lucOS;CTNNB1-Ccl5* mice when compared with *MYC-luc;CTNNB1-Ccl5* mice, suggesting that CCL5 expression restores immune surveillance in the context of β-catenin activation and antigen expression (Fig. 6D and E). Mechanistically, expression of CCL5 in β-catenin–driven tumors led to a significant increase in the levels of DC1 ($DAPI^-CD45^+lin^-MHCII^+CD11c^+CD24^+CD103^+CD11b^-$; Fig. 6F) and antigen-specific $CD8^+$ T cells (Fig. 6G) compared with healthy livers, which could potentially explain the restoration of immune surveillance. As expected, injection of anti-CD4 and anti-CD8 antibodies into *MYC-lucOS;CTNNB1-Ccl5* WT mice led to a decrease in survival when compared with mice treated with control antibodies (Fig. 6H and I). This is similar to the effects seen in DC-deficient *Batf3*$^{-/-}$ mice (Fig. 6J–L) and further confirms the role of CCL5 in mounting an antitumor immune response. In conclusion, CCL5 expression is downregulated in β-catenin–driven murine and human HCCs, and CCL5 reexpression leads to the restoration of the immune surveillance program.

β-Catenin Signaling Activation Confers Resistance to Anti–PD-1 Therapy in HCC

Nivolumab and pembrolizumab, two anti–PD-1 inhibitors, have recently been approved by the FDA for second-line therapy in patients with advanced HCC (6, 7). To test the therapeutic relevance of β-catenin–driven immune escape in response to anti–PD-1, we treated our novel mouse models of HCC with blocking mAbs against murine PD-1. Of note, because most *MYC-lucOS;sg-p53* mice do not develop tumors (Fig. 1E–G), a higher dose of vector DNA was used to force tumor formation. Mice harboring *MYC-lucOS;sg-p53* tumors were responsive to anti–PD-1 treatment (Fig. 7A). In contrast, mice harboring *MYC-luc;sg-p53* tumors did not respond (Fig. 7B), demonstrating that expression of tumor antigens is a requirement for responding to anti–PD-1 therapy. In the case of β-catenin–driven tumors, neither *MYC-lucOS;CTNNB1* or *MYC-luc;CTNNB1* models were responsive to anti–PD-1, proving that β-catenin activation promotes resistance to immunotherapy in our models (Fig. 7C and D).

The association between β-catenin activation and resistance to anti–PD-1 therapy has been observed in patients with HCC (21): None of the 10 patients with HCC with activating mutations in *CTNNB1* had response to anti–PD-1 or anti–PD-L1 therapy whereas 50% of *CTNNB1* WT patients had a response. To test this further, we collected tumor specimens from 15 patients with HCC treated with nivolumab at Mount Sinai Hospital. Overall, 6 (40%) patients responded to anti–PD-1 therapy, with a median survival time of 22.2 months,

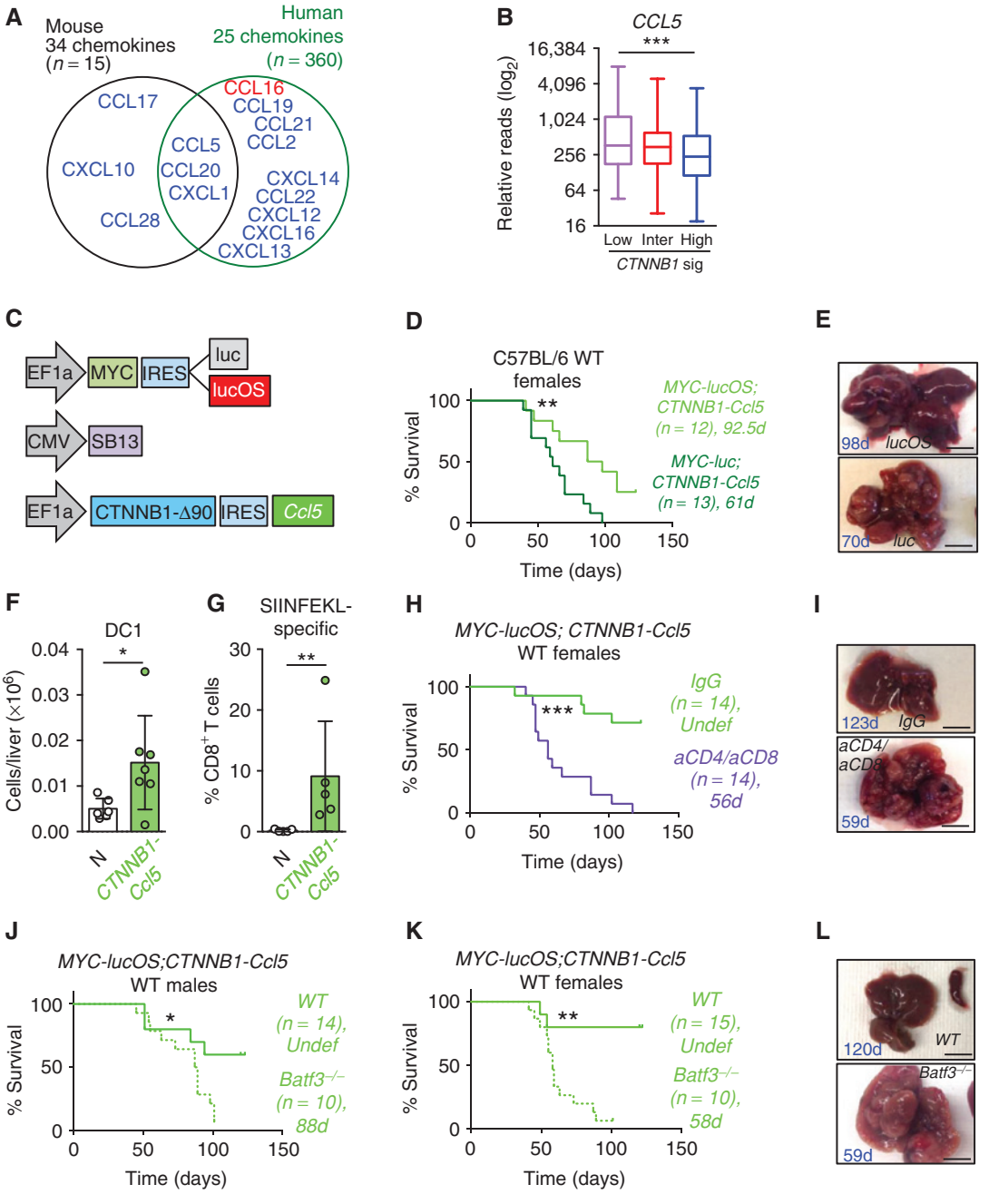

Figure 6. CCL5 expression restores immune surveillance in β-catenin–driven HCCs. **A,** Venn diagram displaying the chemokines differentially expressed in mice or human liver tumors. The number of samples for each dataset is included. Red, significantly upregulated; blue, significantly downregulated. The intersection shows the chemokines dysregulated in both datasets. **B,** Expression of *CCL5* in 360 human HCC samples (LIHC, liver hepatocellular carcinoma, from the TCGA). Box and whisker plot, with the central line representing the median, the ends of the box representing the upper and lower quartiles, and the whiskers extending to the highest and lowest observations. Mann–Whitney test. *CTNNB1* signature low ($n = 120$), intermediate (inter; $n = 120$), and high ($n = 120$). **C,** Schematic of vectors injected into mice. The transposon-based vector overexpressing *CTNNB1* also expresses *Ccl5*. **D,** Survival curves in C57BL/6 WT females. Number of mice per group is shown as well as median survival. Log-rank Mantel–Cox test. **E,** Pictures of representative livers from **D**. The number indicates the number of days from injection to death for that particular mouse. Scale bars, 1 cm. Quantification of the number of DC1 dendritic cells (**F**) or percentage of SIINFEKL-specific $CD8^+$ T cells (**G**) in the livers of the corresponding mice ($n = 5$–7 per group). N, normal liver; *CTNNB1-Ccl5*, *Myc-lucOS;CTNNB1-Ccl5*. Mean and SD are shown. Mann–Whitney test. **H,** Survival curves in C57BL/6 WT females with combined $CD4^+$ and $CD8^+$ T-cell depletion. Number of mice per group is shown as well as median survival. Undef, undefined. Log-rank Mantel–Cox test. **I,** Pictures of representative livers from **F**. The number indicates the number of days from injection to death for that particular mouse. Scale bars, 1 cm. **J** and **K,** Survival curves in C57BL/6 WT or *Batf3*$^{-/-}$ males (**J**) and females (**K**). Number of mice per group is shown as well as median survival. Undef, undefined. Log-rank Mantel–Cox test. **L,** Pictures of representative livers from **K**. The number indicates the number of days from injection to death for that particular mouse. Scale bars, 1 cm. *, $P < 0.05$; **, $P < 0.01$; ***, $P < 0.001$.

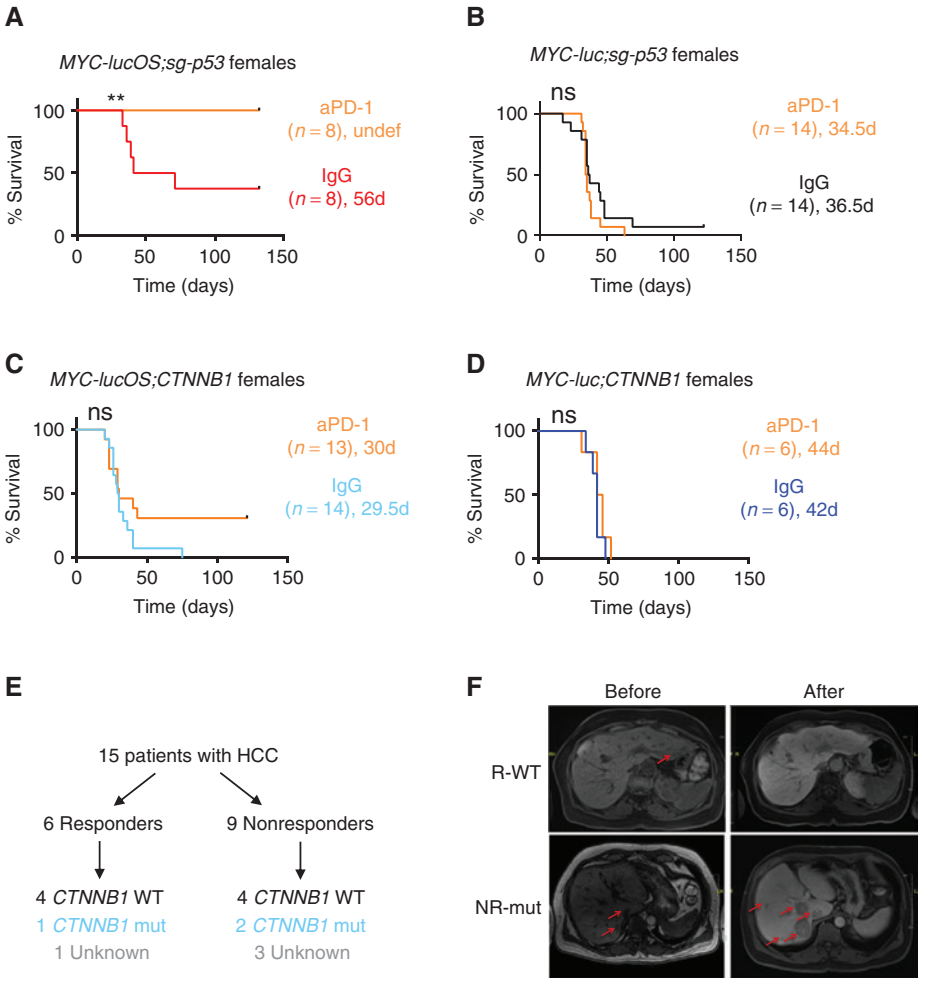

Figure 7. β-catenin signaling activation confers resistance to anti-PD-1 therapy in HCC. Survival curves of C57BL/6 WT females harboring *MYC-lucOS;sg-p53* (**A**), *MYC-luc;sg-p53* (**B**), *MYC-lucOS;CTNNB1* (**C**), or *MYC-luc;CTNNB1* (**D**) tumors treated with control antibodies (IgG) or anti-PD-1 (aPD-1). Number of mice per group is shown as well as median survival. Undef, undefined. Log-rank Mantel–Cox test. **E,** Schematic of patients with HCC treated with nivolumab at Mount Sinai Hospital, including their response and *CTNNB1* mutational status. **F,** Scans of a responder (R; *CTNNB1* WT; top, 6 months) and nonresponder (NR; *CTNNB1* mutated, mut; bottom, 3 months) patient to nivolumab, before and after treatment. Responder shows complete resolution. Nonresponder shows tumor growth and new lesions. **, $P < 0.01$.

and 9 (60%) patients did not respond, with a median survival of 6.2 months ($P = 0.034$; Supplementary Fig. S7A). Of note, 3 patients harbored *CTNNB1* mutations, two being nonresponders and one being a responder (Fig. 7E and F). Because of the small sample size (power calculation of sample size indicates that at least 89 patients would be needed), we were not able to establish statistical significance. Nevertheless, our data together with the previously published study (21) suggest a role for β-catenin in promoting resistance to anti–PD-1 therapy in HCC.

DISCUSSION

In this study, we have demonstrated that β-catenin activation in HCC tumor cells is an important mechanism of immune escape that confers resistance to anti–PD-1 therapies. The use of mAbs directed against inhibitory receptors on immune cells, known as immune checkpoint blockade, has aroused tremendous enthusiasm among clinicians, scientists, and patients (9). In particular, mAbs targeting PD-1/PD-L1 have shown remarkable antitumor activity in numerous malignancies (11, 43–45), leading to their regulatory approval (9). However, despite the unprecedented efficacy of these agents in some patients, the lack of response in the majority emphasizes the pressing need to identify biomarkers that can select the patients that are most likely to benefit from therapy. In other malignancies, mismatch repair deficiency (12, 13), mutations in the SWI/SNF chromatin remodeling complex (46–48), or *ADAR1* mutations (49) sensitize tumors to respond to immunotherapies. In contrast, β-catenin activation (19), *PTEN* deletion (18), or *JAK2* mutations (16) lead to resistance to immunotherapies. Similar studies in HCC have been missing, in part due to the relative delay of the clinical trials testing immunotherapies when compared with other malignancies, such as melanoma or NSCLC. A comprehensive transcriptional

analysis of HCC patient samples has previously found a correlation between *CTNNB1* mutation and T-cell exclusion (20), suggesting that β-catenin activation could be involved in immune escape and resistance to immunotherapies in patients with HCC. This correlation between *CTNNB1* mutation and T-cell exclusion has been validated across a large set of human cancers (50). Furthermore, in a small cohort of patients with HCC, alterations in the β-catenin pathway correlated with lack of response to anti–PD-1 or anti–PD-L1 therapies (21). Here, by using a novel mouse model of HCC, we have functionally shown that β-catenin activation leads to immune exclusion and resistance to anti–PD-1 therapy, which emphasizes the utility of our models to identify processes that are relevant to human disease. One limitation in HCC clinical research is that tumor biopsies are not recommended for patients with advanced HCC (51). A change in the clinical guidelines may be needed to enable liver biopsies in patients with advanced HCC to facilitate the identification of biomarkers of response and implement biomarker-guided therapies.

Mechanistically, we have demonstrated that β-catenin activation in HCC tumor cells impaired recruitment of CD103$^+$ DCs, which are critical cells in mounting an effective antitumor immune response (52). This defective recruitment of DCs in turn impaired the presence of antigen-specific CD8$^+$ T cells in the liver, further confirming the reduced immune surveillance. Interestingly, at an early time point, *CTNNB1*-mutant HCC tumors presented CD8$^+$ T cells that were not antigen-specific and could be bystander T cells (53, 54). However, in murine and human *CTNNB1*-mutant established tumors, T cells were rare, consistent with an immune exclusion phenotype. Moreover, transcriptional analysis of HCC patient samples revealed that transcripts related to DCs and T cells were significantly downregulated in *CTNNB1*-mutant HCC tumors when compared with *CTNNB1* WT tumors, extending our findings to the human setting. A similar observation has been made in melanoma, where β-catenin activation also leads to a defective recruitment of CD103$^+$ DCs (19). In the melanoma study, the reduced recruitment of CD103$^+$ DCs into the tumor microenvironment could partially be explained by a defective production of the chemokine CCL4. In our murine HCC model and in HCC patient samples, chemokine *CCL4* expression levels were unchanged between *CTNNB1*-mutant and *CTNNB1* WT tumor samples. Instead, we found a significant reduction in the levels of chemokines *CXCL1, CCL20*, and *CCL5* in *CTNNB1*-mutant tumors in both murine and human *CTNNB1*-mutant samples. Because CCL5 could potentially affect DCs (42), we decided to further pursue the effect of CCL5 on immune surveillance. Indeed, overexpression of chemokine CCL5 in β-catenin–driven HCC cells led to a higher recruitment of CD103$^+$ DCs, antigen-specific CD8$^+$ T cells, and restoration of immune surveillance, demonstrating its causal role. Restoration of intratumor DCs by intratumor injection of FLT3 ligand–induced bone marrow–derived DCs also had an antitumor effect in melanoma (19). It is striking that in different tumor types, the same signaling pathway, β-catenin activation, elicits a similar mechanism although mediated by different chemokines. It is also possible that additional chemokines and secreted molecules may be involved in the recruitment of DCs in both settings. Nevertheless, therapeutic strategies that promote DC recruitment (55) could improve the response of *CTNNB1*-mutant tumors to anti–PD-1 therapy.

In HCC, around one third of the patients present activating mutations in *CTNNB1* and could potentially be resistant to anti–PD-1 therapies (56). So far, the clinical trials testing nivolumab (6) and pembrolizumab (7) have demonstrated that only around 15% to 20% of patients with HCC exhibit an objective response to these therapies. This suggests that other mechanisms of immune resistance beyond β-catenin activation exist. In fact, in our mouse model, less than 50% of the immune-escaped HCC tumors presented β-catenin activation (as measured by an increase in the expression levels of β-catenin target *Axin2*). Characterization of the remaining tumors has shown that escaped murine liver tumors, which present abundant immune-related transcripts, can escape through different mechanisms. In addition, the temporal study of *MYC-lucOS;sg-p53* tumor cells by single-cell RNA-seq may shed light on the initial changes occurring in tumor cells subjected to immune pressure and undergoing immune surveillance. Single-cell RNA-seq may also enable better establishment of the changes occurring in different cell compartments and the contribution of each compartment to immune escape. Moreover, it is possible that mutations co-occurring with *CTNNB1* mutation may modify the effect that β-catenin activation has in antitumor immunity. In addition, the levels of activation of the β-catenin signaling pathway may affect the phenotype of immune escape. Additional studies will be needed to identify distinct mechanisms of resistance to immunotherapies and refine the set of mutations that cooperate with *CTNNB1* mutation to confer resistance. To address this, it will be critical to combine mechanistic studies in mice with the analysis of HCC patient samples.

To understand the role that different genetic alterations in HCC tumor cells have in immune surveillance and response to immunotherapies, we have generated a novel mouse model of HCC. The model is based on the hydrodynamic tail-vein delivery (30) of genetic elements encoding oncogenes, CRISPR targeting tumor suppressor genes, and exogenous antigens. A similar approach, comparing tumor formation in the absence or presence of exogenous antigen expression, was used to study immune surveillance in lung cancer (29) and to demonstrate immunoediting in the context of sarcoma (17). A recent study in HCC performed hydrodynamic injection of mutant *NRAS, AKT*, and exogenous antigens to demonstrate that antigen-specific T cells undergo exhaustion (57). The strength of our approach is that we can compare the effect that the expression of exogenous antigens has in the context of different genetic alterations, which, coupled with the use of both immunocompetent and immunodeficient mouse models, can lead to fundamental discoveries. For example, performing experiments in the absence or presence of antigens has enabled us to demonstrate that antigen expression in the context of *MYC;Trp53*$^{-/-}$ liver tumors leads to immune surveillance. This strong antitumor immune response is driven by antigen expression and not by the loss of p53, because elimination of immune cells in mice harboring *MYC;Trp53*$^{-/-}$ liver tumors that do not express antigens has no effect. Similarly, antigen expression is critical for responding to anti–PD-1 immunotherapy because mice harboring *MYC;Trp53*$^{-/-}$ liver tumors that do not express antigens are not responsive to

the therapy. The fact that the model antigens are linked to luciferase allows monitoring of tumor growth and immune responses over time by simply performing bioluminescence imaging. However, because the antigens are genetically linked to the driving oncogene, *MYC*, it is likely that there is a selective pressure against the loss of the antigens. The advantage of this may be that the system allows the study of mechanisms of immune escape different from the loss of antigens. It will be interesting to study how HCC-specific tumor antigens, such as α-fetoprotein or glypican 3 (58), instead of model antigens, affect mechanisms of immune surveillance in mice. The benefit of using model antigens, such as the ones used in our study, is that they have the potential to elicit strong immune responses that can be overcome only by bona fide immune escape mechanisms. The temporal control of the expression of the antigens by using inducible systems, uncoupled from the expression of the driving oncogene, may better recapitulate tumor evolution and immune responses. Finally, HCC arises in the context of underlying liver disease. It will be critical to test how different types of liver damage (viral, alcohol-mediated, dietary), which can be easily combined with our model, affect response to immunotherapies.

In conclusion, we provide a novel mouse model of HCC that can be used to identify mechanisms of immune escape and resistance to immunotherapies that are relevant to human disease. This model represents a paradigm of personalized mouse model of HCC that recapitulates immune surveillance and allows interrogation of the role of virtually any genetic alteration in antitumor immunity. With this model, we have found that β-catenin activation promotes immune escape and resistance to anti–PD-1 therapies in HCC. By dissecting the underlying biology, we also propose a mechanism to restore immune surveillance in β-catenin–driven tumors. Finally, our results suggest that *CTNNB1* mutational status could be used as a biomarker for patient exclusion. The identification of additional tumor-intrinsic signaling pathways that disrupt antitumor immunity and affect response to anti–PD-1 by using our novel mouse model may help optimize patient selection.

METHODS

Vector Design and Use

To generate the *pT3-EF1a-MYC-IRES-luciferase* (*MYC-luc*) vector, the *pT3-EF1a-MYC* plasmid was opened with *PmeI* restriction enzyme, the "*IRES-luciferase*" sequence was PCR-amplified from *pMSCV-IRES-luciferase*, and the cloning of the "*IRES-luciferase*" fragment into the linearized *pT3-EF1a-MYC* was performed by using the In-Fusion HD Cloning Plus (Takara Bio). The *pT3-EF1a-MYC-IRES-luciferase-OS* (*MYC-lucOS*) vector was generated by In-Fusion cloning of the *PmeI*-linearized *pT3-EF1a-MYC* vector, the "*IRES-luciferase*" fragment, and the "*OS*" fragment, which was amplified from *Lenti-LucOS* vector by PCR. To generate the *pT3-EF1a-CTNNB1-IRES-Ccl5* vector, the *pT3-EF1a-NRAS-IRES-GFP* plasmid digested with *XhoI* and *EcoRV* restriction enzymes was used as a donor vector. The "*CTNNB1*," "*IRES*," and "*Ccl5*" sequences were PCR-amplified from the *pT3-N90-CTNNB1*, the *pT3-EF1a-NRAS-IRES-GFP,* and the *pMD-mCcl5* plasmids, respectively, and the cloning of the three fragments into the donor vector was performed by In-Fusion cloning. The *CMV-SB13, pT3-EF1a-NRAS-IRES-GFP,* and *pMSCV-IRES-luciferase* plasmids were kindly provided by Dr. Scott Lowe (Memorial Sloan Kettering Cancer Center, New York, NY). The *pT3-EF1a-MYC* and *pT3-N90-CTNNB1* (Addgene plasmid #31785) were a kind gift from Dr. Xin Chen (University of California, San Francisco, CA). *Lenti-LucOS* (Addgene plasmid #22777) was a gift from Dr. Tyler Jacks. The full-length cDNA of *Ccl5* was obtained from Sino Biological (plasmid reference: MG50022-M). The *px330-sg-p53* was previously published and validated (31). The *px330* vector was a gift from Feng Zhang (Addgene plasmid #42230). All constructs were verified by nucleotide sequencing and vector integrity was confirmed by restriction enzyme digestion. The new vectors will be made available through Addgene.

Hydrodynamic Tail-Vein Injection

A sterile 0.9% NaCl solution/plasmid mix was prepared containing DNA. We prepared 11.4 μg of *pT3-EF1a-MYC-IRES-luciferase* (*MYC-luc*), 12 μg of *pT3-EF1a-MYC-IRES-luciferase-OS* (*MYC-lucOS*), 10 μg of *pT3-N90-CTNNB1* (*CTNNB1*), 27 μg of *pT3-EF1a-CTNNB1-IRES-Ccl5* (*CTNNB1-Ccl5*), 10 μg of *px330-sg-p53* (*sg-p53*), and a 4:1 ratio of transposon to *SB13* transposase–encoding plasmid dissolved in 2 mL of 0.9% NaCl solution and injected 10% of the weight of each mouse in volume. Because two independent "hits" are required for tumor formation in C57BL/6 mice (30), only those hepatocytes that receive the three plasmids (transposon-based, transposase, and CRISPR-based) will have the potential to form tumors. We also show that a single hepatocyte can take up to four plasmids, as shown in *MYC-lucOS;CTNNB1;sg-p53* tumors. For the anti–PD-1 experiment, we used 13 μg of *pT3-EF1a-MYC-IRES-luciferase-OS,* 13 μg of *px330-sg-p53* (*sg-p53*), and a 4:1 ratio of transposon to *SB13* transposase–encoding plasmid per 2 mL. Mice were injected with the 0.9% NaCl solution/plasmid mix into the lateral tail vein with a total volume corresponding to 10% of body weight in 5 to 7 seconds. Vectors for hydrodynamic delivery were produced using the QIAGEN plasmid *Plus*Mega kit (QIAGEN). Equivalent DNA concentration between different batches of DNA was confirmed to ensure reproducibility among experiments.

Mice

Different batches of WT C57BL/6 mice were purchased from Envigo and were used for the treatment experiments (with mAbs) or for flow cytometry experiments. *Rag2*$^{-/-}$ and *Batf3*$^{-/-}$ mice in C57BL/6 background were obtained from Jackson Laboratories and bred at Icahn School of Medicine at Mount Sinai (ISMMS). Controls for *Rag2*$^{-/-}$ and *Batf3*$^{-/-}$ mice were WT C57BL/6 mice purchased from Jackson and bred at ISMMS. All mouse experiments were approved by the ISMMS Animal Care and Use Committee (protocol number IACUC-2014-0229). Mice were maintained under specific pathogen-free conditions, and food and water were provided *ad libitum*. All animals were examined prior to the initiation of the studies to ensure that they were healthy and acclimated to the laboratory environment. All experiments were performed with 6- to 8-week-old mice, and both males and females were used in most experiments (analyzed separately). Once the animals were sacrificed, livers were collected, formalin-fixed and paraffin-embedded, frozen, or embedded in OCT (Tissue Tek).

Deep Sequencing of CRISPR-Modified Trp53 Locus

The genomic region of *Trp53* targeted by *sg-p53* was PCR amplified using Platinum SuperFi (Invitrogen) high-fidelity DNA polymerase and PCR purified. The primers used were 5′-AAGCCATAGGGGTTT GTTTG-3′ (forward) and 5′-GATACAGGTATGGCGGGATG-3′ (reverse). Libraries were made from 500 ng of the PCR products using the Nextera protocol and sequenced on Illumina MiSeq (250 base pair paired-end). Data were processed according to standard Illumina sequencing analysis procedures. The raw Illumina reads were checked for adapters and quality via FastQC. The raw Illumina sequence reads were trimmed of their adapters and nucleotides with poor quality using Trimmomatic v. 0.36. Paired sequence reads were then merged to form a single sequence if the forward and reverse reads were able

to overlap. The merged reads were aligned to the reference sequence using bwa version 0.7.12, and variant detection was performed using GENEWIZ proprietary Amplicon-EZ program. Two to four biological replicates were sequenced for *in vivo* liver samples.

Treatments

Treatments were initiated one week after the hydrodynamic delivery of the plasmids, a time point that already presents malignant tumor cells. For the experiments with anti–PD-1 mAbs, three doses of either anti–PD-1 (200 μg, clone RMP1-14, BioXcell) or IgG (200 μg, IgG2b, clone LTF-2, BioXcell) were given intraperitoneally at days 7, 9, and 11. For the T-cell depletion experiments, mice were injected intraperitoneally with anti-CD4 (200 μg, clone GK1.5, BioXcell), anti-CD8 (200 μg, clone 2.43, BioXcell), or IgG (200 μg, IgG2b, clone LTF-2, BioXcell) at days 7, 9, 11, and 13, and then once weekly until the end of the experiment. For the combined depletion of $CD4^+$ and $CD8^+$ T cells, 200 μg of each antibody were used and 400 μg of IgG.

Luciferase Detection

In vivo bioluminescence imaging was performed using an IVIS Spectrum system (Caliper LifeSciences, purchased with the support of NCRR S10-RR026561-01) to quantify liver tumor burden before being evenly assigned to various treatment study cohorts. Mice were imaged 5 minutes after intraperitoneal injection with fresh D-luciferin (150 mg/kg; Thermo Fisher Scientific). Luciferase signal was quantified using Living Image software (Caliper LifeSciences). Normalized luciferase signal was calculated by subtracting the background signal. Each treatment cohort had equivalent average luciferase signal. Those mice with a luciferase signal a log of magnitude lower than the average signal were excluded from the study.

RNA-seq and Analysis

RNA was poly-A selected, and multiplexed RNA-seq libraries were prepared using the TruSeq RNA Sample Preparation kit (Illumina) according to the manufacturer's instructions at the ISMMS Genomics Core. The libraries were quantified using the Qubit Broad Range kit (Thermo Fisher Scientific) and sequenced using the Illumina HiSeq 4000 system (SR100). The RNA-seq data was analyzed using Basepair software (www.basepairtech.com) with a pipeline that included the following steps. Reads were aligned to the transcriptome derived from UCSC genome assembly mm10 using Tophat2 with default parameters. Read counts for each transcript were measured using featureCounts (59). Differentially expressed genes were determined using DESeq2 (60) and a cutoff of 0.05 on adjusted *P* value (corrected for multiple hypotheses testing) was used for creating gene lists. GSEA was performed on normalized gene expression counts, using gene permutations for calculating *P* value, to characterize the molecular alterations enriched between different groups (34). GSEA, FDR value < 0.25, and $P < 0.05$ (as accepted). The files can be found at GEO (GSE125336).

Human HCC Sample Analysis

MYC, TP53, and *CTNNB1* genomic alterations in patients with HCC ($n = 366$) were obtained from the cBioPortal (61) TCGA dataset. Gene expression profiling of a total of 360 human samples was extracted from the TCGA (December 2018). Samples were stratified depending on *CTNNB1* status as WT or mutant, or *CTNNB1*-mutant HCC gene signature enrichment levels (in tertiles). Mann–Whitney test was performed to test for differences in gene expression values on the log scale.

Patient Cohort and Evaluation of Treatment Response

Patients receiving nivolumab at ISMMS were eligible to be enrolled in the study if they had a confirmed histologic diagnosis of HCC and viable tumor tissue (either biopsy or archival sample) prior to the start of immunotherapy. Once local Institutional Review Board (IRB) approval was granted, written informed consent for tumor profiling was obtained from each patient on a retrospective protocol (IRB number 17-01728) in accordance with the Belmont Report. Initial diagnosis of HCC was made following the clinical practice guidelines from the European Association for the Study of the Liver (62). All included patients presented an advanced (BCLC-C) or intermediate (BCLC-B) stage with prior progression to surgery and/or locoregional therapies at the moment of immunotherapy initiation. Nivolumab was administered at a dose of 240 mg every 2 weeks and was continued until toxicity, progression, or death, according to the treating physician. Assessment of response was conducted at least 3 months after treatment initiation and performed by mRECIST criteria (63). Treatment response was defined as follows: complete response (CR; disappearance of any intratumor arterial enhancement in all target lesions); partial response (PR; at least a 30% decrease in the sum of diameters of viable (enhancement in the arterial phase) target lesions, taking as reference the baseline sum of the diameters of target lesions); progressive disease [PD; an increase of at least 20% in the sum of the diameters of viable (enhancing) target lesions, taking as reference the smallest sum of the diameters of viable (enhancing) target lesions recorded since treatment started]; stable disease (SD; any cases not qualifying for either PR or PD). The electronic medical records were reviewed to extract information on patient's gender, age, race, etiology, date of diagnosis, specimen location (liver, local recurrence, or extrahepatic metastasis), extent of disease, treatment history, type, number and dates of systemic therapy with radiographic response, date of progression, and the last date of follow-up or date of death.

Statistical Analysis

Data are expressed as mean ± SD. Statistical significance was determined using Mann–Whitney *U* test (when $n < 10$ or nonnormal distribution) or Student *t* test ($n > 10$ and normal distribution). For comparisons of more than two groups, we used ANOVA test. For paired comparisons, we used the Wilcoxon test. For frequency comparisons, we utilized the χ^2 test. Group size was determined on the basis of the results of preliminary experiments, and no statistical method was used to predetermine sample size. Group allocation for treatments was performed to ensure equivalent luciferase signal, and outcome assessment was not performed in a blinded manner. The differences in survival were calculated using the Kaplan–Meier test. GraphPad Prism 6 software was used to create the graphs and for the statistical analysis. Significance values were set at *, $P < 0.05$; **, $P < 0.01$; ***, $P < 0.001$.

The rest of materials and methods can be found in Supplementary Methods.

Disclosure of Potential Conflicts of Interest

A. Villanueva is a consultant/advisory board member for Guidepoint, Fujifilm, Exact Sciences, Nucleix, NGM Pharmaceuticals, and Exelixis. J.M. Llovet reports receiving commercial research grants from Bayer Healthcare Pharmaceuticals, Eisai Inc., Bristol-Myers Squibb, and IPSEN, and is a consultant/advisory board member for Eli Lilly, Bayer HealthCare Pharmaceuticals, Navigant, Leerink Swann LLC, Midatech Ltd., Fortress Biotech Inc., Spring Bank Pharmaceuticals, Nucleix, Can-Fite Biopharma, Bristol-Myers Squibb, Eisai Inc., Celsion, Exelixis, Merck, Blueprint, Ipsen, and Glycotest. A. Lujambio reports receiving commercial research grants from Pfizer and Genentech and has received speakers bureau honoraria from Exelixis. No potential conflicts of interest were disclosed by the other authors.

Authors' Contributions

Conception and design: M. Ruiz de Galarreta, A. Lujambio
Development of methodology: M. Ruiz de Galarreta, K.E. Lindblad, M. Casanova-Acebes, A. Lujambio

Acquisition of data (provided animals, acquired and managed patients, provided facilities, etc.): M. Ruiz de Galarreta, E. Bresnahan, P. Molina-Sánchez, K.E. Lindblad, B. Maier, D. Sia, M. Puigvehi, V. Miguela, M. Casanova-Acebes, M. Dhainaut, A.D. Singhi, A. Moghe, J. von Felden, L. Tal Grinspan, S. Wang, S.P. Monga, B.D. Brown, J.M. Llovet, M. Merad
Analysis and interpretation of data (e.g., statistical analysis, biostatistics, computational analysis): M. Ruiz de Galarreta, E. Bresnahan, P. Molina-Sánchez, K.E. Lindblad, B. Maier, D. Sia, M. Puigvehi, V. Miguela, M. Casanova-Acebes, M. Dhainaut, C. Villacorta-Martin, J. von Felden, L. Tal Grinspan, S. Wang, A.O. Kamphorst, S.P. Monga, A. Villanueva, J.M. Llovet, A. Lujambio
Writing, review, and/or revision of the manuscript: M. Ruiz de Galarreta, E. Bresnahan, P. Molina-Sánchez, K.E. Lindblad, B. Maier, D. Sia, M. Puigvehi, V. Miguela, M. Casanova-Acebes, M. Dhainaut, C. Villacorta-Martin, A.D. Singh, A. Moghe, J. von Felden, L. Tal Grinspan, S. Wang, A.O. Kamphorst, S.P. Monga, B.D. Brown, A. Villanueva, J.M. Llovet, M. Merad, A. Lujambio
Administrative, technical, or material support (i.e., reporting or organizing data, constructing databases): M. Ruiz de Galarreta, E. Bresnahan, P. Molina-Sánchez, K.E. Lindblad, M. Puigvehi, A. Moghe, J. von Felden, L. Tal Grinspan, A. Villanueva
Study supervision: M. Ruiz de Galarreta, A. Lujambio

Acknowledgments

We wish to thank the patients who generously provided tissues and participated in our studies. We thank Drs. Scott Lowe, Xin Chen, Tyler Jacks, and Feng Zhang for access to plasmids. We thank the Center for Comparative Medicine and Surgery (CCMS), the Tisch Cancer Institute Flow Cytometry Shared Resource Facility, the ISMMS Oncological Sciences Histology Shared Resource Facility, ISMMS Genomics Core Facility, the Translational and Molecular Imaging Institute (TMII) Imaging Core, and the ISMMS Biorepository and Pathology Core. We thank Drs. Scott L. Friedman, Joshua Brody, and Andriana Kotini for insightful comments. M. Ruiz de Galarreta was supported by the Fundación Alfonso Martín Escudero Fellowship and the Damon Runyon-Rachleff Innovation Award (DR52-18). E. Bresnahan was supported by the Damon Runyon-Rachleff Innovation Award (DR52-18). P. Molina-Sánchez was supported by a Pfizer Research Grant and the NIH/NCI R37 Merit Award (R37CA230636). K.E. Lindblad was supported by the NIH/NCI R37 Merit Award (R37CA230636) and the Graduate School of Biomedical Sciences at ISMMS. B. Maier was supported by the NIH/NIAID R56AI137244 grant. D. Sia was supported by the Gilead Science Research Scholar in Liver Diseases. M. Puigvehi received a scholarship grant from the Asociación Española para el Estudio del Hígado (AEEH). V. Miguela was supported by Department of Defense (DoD) Career Development Award (CA150178) and DoD Translational Team Science Award (CA150272P2). M. Casanova-Acebes was supported by the Long-Term Human Frontiers Science Program (LT00110/2015-L/1). M. Dhainaut was supported by the Belgian American Educational Foundation. C. Villacorta-Martin was supported by the DoD Translational Team Science Award (CA150272P3). J. von Felden is supported by the German Research Foundation (FE 1746/1-1). S.P. Monga was supported by NIH grant R01CA204586 and the Endowed Chair for Experimental Pathology. A. Villanueva was supported by the DoD Translational Team Science Award (CA150272P3). B.D. Brown was supported by R33CA223947. J.M. Llovet was supported by the NCI (P30-CA196521), the DoD Translational Team Science Award (CA150272P1), the European Commission (EC)/Horizon 2020 Program (HEPCAR, Ref. 667273-2), EIT Health (CRISH2, Ref. 18053), the Accelerator Award (CRUCK, AEEC, AIRC; HUNTER, Ref. C9380/A26813), the Samuel Waxman Cancer Research Foundation, Spanish National Health Institute (SAF2016-76390), and the Generalitat de Catalunya/AGAUR (SGR-1358). M. Merad was supported by NIH/NIAID (U19AI128949). A. Lujambio was supported by a Damon Runyon-Rachleff Innovation Award (DR52-18), R37 Merit Award (R37CA230636), DoD Career Development Award (CA150178), DoD Translational Team Science Award (CA150272P2), and the Icahn School of Medicine at Mount Sinai. The Tisch Cancer Institute and related research facilities are supported by P30 CA196521.

The costs of publication of this article were defrayed in part by the payment of page charges. This article must therefore be hereby marked *advertisement* in accordance with 18 U.S.C. Section 1734 solely to indicate this fact.

Received January 18, 2019; revised May 13, 2019; accepted June 7, 2019; published first June 11, 2019.

REFERENCES

1. Llovet JM, Montal R, Sia D, Finn RS. Molecular therapies and precision medicine for hepatocellular carcinoma. Nat Rev Clin Oncol 2018;15:599–616.
2. Llovet JM, Ricci S, Mazzaferro V, Hilgard P, Gane E, Blanc JF, et al. Sorafenib in advanced hepatocellular carcinoma. N Engl J Med 2008;359:378–90.
3. Kudo M, Finn RS, Qin S, Han KH, Ikeda K, Piscaglia F, et al. Lenvatinib versus sorafenib in first-line treatment of patients with unresectable hepatocellular carcinoma: a randomised phase 3 non-inferiority trial. Lancet 2018;391:1163–73.
4. Bruix J, Qin S, Merle P, Granito A, Huang YH, Bodoky G, et al. Regorafenib for patients with hepatocellular carcinoma who progressed on sorafenib treatment (RESORCE): a randomised, double-blind, placebo-controlled, phase 3 trial. Lancet 2017;389:56–66.
5. Abou-Alfa GK, Meyer T, Cheng AL, El-Khoueiry AB, Rimassa L, Ryoo BY, et al. Cabozantinib in patients with advanced and progressing hepatocellular carcinoma. N Engl J Med 2018;379:54–63.
6. El-Khoueiry AB, Sangro B, Yau T, Crocenzi TS, Kudo M, Hsu C, et al. Nivolumab in patients with advanced hepatocellular carcinoma (CheckMate 040): an open-label, non-comparative, phase 1/2 dose escalation and expansion trial. Lancet 2017;389:2492–502.
7. Zhu AX, Finn RS, Edeline J, Cattan S, Ogasawara S, Palmer D, et al. Pembrolizumab in patients with advanced hepatocellular carcinoma previously treated with sorafenib (KEYNOTE-224): a non-randomised, open-label phase 2 trial. Lancet Oncol 2018;19:940–52.
8. Sharma P, Hu-Lieskovan S, Wargo JA, Ribas A. Primary, adaptive, and acquired resistance to cancer immunotherapy. Cell 2017;168:707–23.
9. Ott PA, Hodi FS, Kaufman HL, Wigginton JM, Wolchok JD. Combination immunotherapy: a road map. J Immunother Cancer 2017;5:16.
10. Larkin J, Chiarion-Sileni V, Gonzalez R, Grob JJ, Cowey CL, Lao CD, et al. Combined nivolumab and ipilimumab or monotherapy in untreated melanoma. N Engl J Med 2015;373:23–34.
11. Garon EB, Rizvi NA, Hui R, Leighl N, Balmanoukian AS, Eder JP, et al. Pembrolizumab for the treatment of non-small-cell lung cancer. N Engl J Med 2015;372:2018–28.
12. Le DT, Uram JN, Wang H, Bartlett BR, Kemberling H, Eyring AD, et al. PD-1 blockade in tumors with mismatch-repair deficiency. N Engl J Med 2015;372:2509–20.
13. Le DT, Durham JN, Smith KN, Wang H, Bartlett BR, Aulakh LK, et al. Mismatch-repair deficiency predicts response of solid tumors to PD-1 blockade. Science 2017;357:409–13.
14. Rizvi NA, Hellmann MD, Snyder A, Kvistborg P, Makarov V, Havel JJ, et al. Cancer immunology. Mutational landscape determines sensitivity to PD-1 blockade in non-small cell lung cancer. Science 2015;348:124–8.
15. Snyder A, Makarov V, Merghoub T, Yuan J, Zaretsky JM, Desrichard A, et al. Genetic basis for clinical response to CTLA-4 blockade in melanoma. N Engl J Med 2014;371:2189–99.
16. Zaretsky JM, Garcia-Diaz A, Shin DS, Escuin-Ordinas H, Hugo W, Hu-Lieskovan S, et al. Mutations associated with acquired resistance to PD-1 blockade in melanoma. N Engl J Med 2016;375:819–29.
17. DuPage M, Mazumdar C, Schmidt LM, Cheung AF, Jacks T. Expression of tumour-specific antigens underlies cancer immunoediting. Nature 2012;482:405–9.

18. Peng W, Chen JQ, Liu C, Malu S, Creasy C, Tetzlaff MT, et al. Loss of PTEN promotes resistance to T cell-mediated immunotherapy. Cancer Discov 2016;6:202–16.
19. Spranger S, Bao R, Gajewski TF. Melanoma-intrinsic beta-catenin signalling prevents anti-tumour immunity. Nature 2015;523:231–5.
20. Sia D, Jiao Y, Martinez-Quetglas I, Kuchuk O, Villacorta-Martin C, Castro de Moura M, et al. Identification of an immune-specific class of hepatocellular carcinoma, based on molecular features. Gastroenterology 2017;153:812–26.
21. Harding JJ, Nandakumar S, Armenia J, Khalil DN, Albano M, Ly M, et al. Prospective genotyping of hepatocellular carcinoma: clinical implications of next generation sequencing for matching patients to targeted and immune therapies. Clin Cancer Res 2018;25:2116–26.
22. Zitvogel L, Pitt JM, Daillere R, Smyth MJ, Kroemer G. Mouse models in oncoimmunology. Nat Rev Cancer 2016;16:759–73.
23. Brown ZJ, Heinrich B, Greten TF. Mouse models of hepatocellular carcinoma: an overview and highlights for immunotherapy research. Nat Rev Gastroenterol Hepatol 2018;15:536–54.
24. Ochsenbein AF, Sierro S, Odermatt B, Pericin M, Karrer U, Hermans J, et al. Roles of tumour localization, second signals and cross priming in cytotoxic T-cell induction. Nature 2001;411:1058–64.
25. Spiotto MT, Rowley DA, Schreiber H. Bystander elimination of antigen loss variants in established tumors. Nat Med 2004;10:294–8.
26. Dunn GP, Bruce AT, Ikeda H, Old LJ, Schreiber RD. Cancer immunoediting: from immunosurveillance to tumor escape. Nat Immunol 2002;3:991–8.
27. Frese KK, Tuveson DA. Maximizing mouse cancer models. Nat Rev Cancer 2007;7:645–58.
28. Drake CG, Doody AD, Mihalyo MA, Huang CT, Kelleher E, Ravi S, et al. Androgen ablation mitigates tolerance to a prostate/prostate cancer-restricted antigen. Cancer Cell 2005;7:239–49.
29. DuPage M, Cheung AF, Mazumdar C, Winslow MM, Bronson R, Schmidt LM, et al. Endogenous T cell responses to antigens expressed in lung adenocarcinomas delay malignant tumor progression. Cancer Cell 2011;19:72–85.
30. Chen X, Calvisi DF. Hydrodynamic transfection for generation of novel mouse models for liver cancer research. Am J Pathol 2014;184:912–23.
31. Bollard J, Miguela V, Ruiz de Galarreta M, Venkatesh A, Bian CB, Roberto MP, et al. Palbociclib (PD-0332991), a selective CDK4/6 inhibitor, restricts tumour growth in preclinical models of hepatocellular carcinoma. Gut 2017;66:1286–96.
32. Limberis MP, Bell CL, Wilson JM. Identification of the murine firefly luciferase-specific CD8 T-cell epitopes. Gene Ther 2009;16:441–7.
33. Xue W, Chen S, Yin H, Tammela T, Papagiannakopoulos T, Joshi NS, et al. CRISPR-mediated direct mutation of cancer genes in the mouse liver. Nature 2014;514:380–4.
34. Subramanian A, Tamayo P, Mootha VK, Mukherjee S, Ebert BL, Gillette MA, et al. Gene set enrichment analysis: a knowledge-based approach for interpreting genome-wide expression profiles. Proc Natl Acad Sci U S A 2005;102:15545–50.
35. Liberzon A, Subramanian A, Pinchback R, Thorvaldsdottir H, Tamayo P, Mesirov JP. Molecular signatures database (MSigDB) 3.0. Bioinformatics 2011;27:1739–40.
36. Chiang DY, Villanueva A, Hoshida Y, Peix J, Newell P, Minguez B, et al. Focal gains of VEGFA and molecular classification of hepatocellular carcinoma. Cancer Res 2008;68:6779–88.
37. Cancer Genome Atlas Research Network. Comprehensive and integrative genomic characterization of hepatocellular carcinoma. Cell 2017;169:1327–41.
38. Schulze K, Imbeaud S, Letouze E, Alexandrov LB, Calderaro J, Rebouissou S, et al. Exome sequencing of hepatocellular carcinomas identifies new mutational signatures and potential therapeutic targets. Nat Genet 2015;47:505–11.
39. Tward AD, Jones KD, Yant S, Cheung ST, Fan ST, Chen X, et al. Distinct pathways of genomic progression to benign and malignant tumors of the liver. Proc Natl Acad Sci U S A 2007;104:14771–6.
40. Ang C, Miura JT, Gamblin TC, He R, Xiu J, Millis SZ, et al. Comprehensive multiplatform biomarker analysis of 350 hepatocellular carcinomas identifies potential novel therapeutic options. J Surg Oncol 2016;113:55–61.
41. Hildner K, Edelson BT, Purtha WE, Diamond M, Matsushita H, Kohyama M, et al. Batf3 deficiency reveals a critical role for CD8alpha+ dendritic cells in cytotoxic T cell immunity. Science 2008;322:1097–100.
42. Chabot V, Reverdiau P, Iochmann S, Rico A, Senecal D, Goupille C, et al. CCL5-enhanced human immature dendritic cell migration through the basement membrane in vitro depends on matrix metalloproteinase-9. J Leukoc Biol 2006;79:767–78.
43. Lipson EJ, Sharfman WH, Drake CG, Wollner I, Taube JM, Anders RA, et al. Durable cancer regression off-treatment and effective reinduction therapy with an anti-PD-1 antibody. Clin Cancer Res 2013;19:462–8.
44. Brahmer JR, Tykodi SS, Chow LQ, Hwu WJ, Topalian SL, Hwu P, et al. Safety and activity of anti-PD-L1 antibody in patients with advanced cancer. N Engl J Med 2012;366:2455–65.
45. Topalian SL, Hodi FS, Brahmer JR, Gettinger SN, Smith DC, McDermott DF, et al. Safety, activity, and immune correlates of anti-PD-1 antibody in cancer. N Engl J Med 2012;366:2443–54.
46. Pan D, Kobayashi A, Jiang P, Ferrari de Andrade L, Tay RE, Luoma AM, et al. A major chromatin regulator determines resistance of tumor cells to T cell-mediated killing. Science 2018;359:770–5.
47. Miao D, Margolis CA, Gao W, Voss MH, Li W, Martini DJ, et al. Genomic correlates of response to immune checkpoint therapies in clear cell renal cell carcinoma. Science 2018;359:801–6.
48. Shen J, Ju Z, Zhao W, Wang L, Peng Y, Ge Z, et al. ARID1A deficiency promotes mutability and potentiates therapeutic antitumor immunity unleashed by immune checkpoint blockade. Nat Med 2018;24:556–62.
49. Ishizuka JJ, Manguso RT, Cheruiyot CK, Bi K, Panda A, Iracheta-Vellve A, et al. Loss of ADAR1 in tumours overcomes resistance to immune checkpoint blockade. Nature 2018;565:43–8.
50. Luke JJ, Bao R, Sweis RF, Spranger S, Gajewski TF. WNT/beta-catenin pathway activation correlates with immune exclusion across human cancers. Clin Cancer Res 2019;25:3074–83.
51. Finn RS. The role of liver biopsy in hepatocellular carcinoma. Gastroenterol Hepatol 2016;12:628–30.
52. Salmon H, Idoyaga J, Rahman A, Leboeuf M, Remark R, Jordan S, et al. Expansion and activation of CD103(+) dendritic cell progenitors at the tumor site enhances tumor responses to therapeutic PD-L1 and BRAF inhibition. Immunity 2016;44:924–38.
53. Simoni Y, Becht E, Fehlings M, Loh CY, Koo SL, Teng KWW, et al. Bystander CD8(+) T cells are abundant and phenotypically distinct in human tumour infiltrates. Nature 2018;557:575–9.
54. Scheper W, Kelderman S, Fanchi LF, Linnemann C, Bendle G, de Rooij MAJ, et al. Low and variable tumor reactivity of the intratumoral TCR repertoire in human cancers. Nat Med 2019;25:89–94.
55. Hammerich L, Marron TU, Upadhyay R, Svensson-Arvelund J, Dhainaut M, Hussein S, et al. Systemic clinical tumor regressions and potentiation of PD1 blockade with in situ vaccination. Nat Med 2019;25:814–24.
56. Pinyol R, Sia D, Llovet JM. Immune exclusion-Wnt/CTNNB1 class predicts resistance to immunotherapies in HCC. Clin Cancer Res 2019;25:2021–3.
57. Liu YT, Tseng TC, Soong RS, Peng CY, Cheng YH, Huang SF, et al. A novel spontaneous hepatocellular carcinoma mouse model for studying T-cell exhaustion in the tumor microenvironment. J Immunother Cancer 2018;6:144.
58. Prieto J, Melero I, Sangro B. Immunological landscape and immunotherapy of hepatocellular carcinoma. Nat Rev Gastroenterol Hepatol 2015;12:681–700.
59. Liao Y, Smyth GK, Shi W. featureCounts: an efficient general purpose program for assigning sequence reads to genomic features. Bioinformatics 2014;30:923–30.
60. Love MI, Huber W, Anders S. Moderated estimation of fold change and dispersion for RNA-seq data with DESeq2. Genome Biol 2014;15:550.
61. Cerami E, Gao J, Dogrusoz U, Gross BE, Sumer SO, Aksoy BA, et al. The cBio cancer genomics portal: an open platform for exploring multidimensional cancer genomics data. Cancer Discov 2012;2:401–4.
62. European Association for the Study of the Liver. EASL Clinical Practice Guidelines: management of hepatocellular carcinoma. J Hepatol 2018;69:182–236.
63. Lencioni R, Llovet JM. Modified RECIST (mRECIST) assessment for hepatocellular carcinoma. Semin Liver Dis 2010;30:52–60.